PROPAGATION OF MULTIWAVELENGTH LASER RADIATION THROUGH ATMOSPHERIC TURBULENCE

J. Richard Kerr

Oregon Graduate Center for Study and Research

Prepared for:

Rome Air Development Center
Advanced Research Projects Agency

August 1973

RADC-TR-73-322
Final Technical Report
August 1973

PROPAGATION OF MULTIWAVELENGTH LASER RADIATION THROUGH ATMOSPHERIC TURBULENCE

Oregon Graduate Center for Study and Research

Sponsored by
Defense Advanced Research Projects Agency
ARPA Order No. 1279, Amend. 5

Rome Air Development Center
Air Force Systems Command
Griffiss Air Force Base, New York

UNCLASSIFIED

SECURITY CLASSIFICATION OF THIS PAGE *(When Data Entered)*

REPORT DOCUMENTATION PAGE		READ INSTRUCTIONS BEFORE COMPLETING FORM
1. REPORT NUMBER RADC-TR-73-322	2. GOVT ACCESSION NO.	3. RECIPIENT'S CATALOG NUMBER
4. TITLE *(and Subtitle)* Propagation of Multiwavelength Laser Radiation Through Atmospheric Turbulence		5. TYPE OF REPORT & PERIOD COVERED Technical Report (15 Jun 72 - 31 Aug 73) 6. PERFORMING ORG. REPORT NUMBER 1174-4
7. AUTHOR(s) J. Richard Kerr		8. CONTRACT OR GRANT NUMBER(s) F30602-72-C-0470
9. PERFORMING ORGANIZATION NAME AND ADDRESS Orego. Graduate Center for Study & Research 19600 N.W. Walker Rd. Beaverton OR 97005		10. PROGRAM ELEMENT, PROJECT, TASK AREA & WORK UNIT NUMBERS 62301E, 1279, 02, 07
11. CONTROLLING OFFICE NAME AND ADDRESS Defense Advanced Research Projects Agency Washington DC 20301		12. REPORT DATE August 1973 13. NUMBER OF PAGES 72
14. MONITORING AGENCY NAME & ADDRESS*(if different from Controlling Office)* RADC (OCSE) Griffiss AFB NY 13441		15. SECURITY CLASS. *(of this report)* Uncl 15a. DECLASSIFICATION/DOWNGRADING SCHEDULE N/A

16. DISTRIBUTION STATEMENT *(of this Report)*

Approved for public release; distribution unlimited

17. DISTRIBUTION STATEMENT *(of the abstract entered in Block 20, if different from Report)*

18. SUPPLEMENTARY NOTES

19. KEY WORDS *(Continue on reverse side if necessary and identify by block number)*

propagation
turbulence
atmospheric optics
scintillation
10.6 microns

20. ABSTRACT *(Continue on reverse side if necessary and identify by block number)*

Finite-beam experiments are being conducted with a wander-cancelling, tracking-transmitter over a 1.6 km, uniform path. A new prediction is given for the transverse amplitude correlation length under near field conditions in strong turbulence. A useful, physically derived approximation to combined diffraction, wander, and short-term-beamspread angles or mean target irradiance is presented, and shown to agree well with more rigorous numerical calculations; experiments under strong turbulence conditions show a

DD FORM 1 JAN 73 1473 EDITION OF 1 NOV 65 IS OBSOLETE

UNCLASSIFIED

SECURITY CLASSIFICATION OF THIS PAGE *(When Data Entered)*

20. substantial and surprising advantage for wander-tracking. The normalized variance of the fluctuating irradiance (strength of fading) due to scintillation, wander, and coherent fading is also discussed, and probability distributions and spectra of wander and irradiance are presented.

Microthermal fluctuations due to turbulence are considered, and it is shown experimentally that the statistics of appropriately averaged first-increments or derivatives behave in accordance with recent theoretical predictions. Short-term turbulence and scintillation statistics are discussed, including intermittency effects. It is pointed out that the level-crossing and conditional probability problems for the scintillating irradiance are complicated by the non-Markovian nature of this process.

PROPAGATION OF MULTIWAVELENGTH LASER RADIATION THROUGH ATMOSPHERIC TURBULENCE

Dr. J. Richard Kerr

Contractor: Oregon Graduate Center for Study and Research
Contract Number: F30602-72-C-0470
Effective Date of Contract: 15 June 1972
Contract Expiration Date: 31 August 1973
Amount of Contract: $75,682.00
Program Code Number: 3E20

Principal Investigator: Dr. J. Richard Kerr
Phone: 503 645-1121

Project Engineer: Mr. Raymond P. Urtz, Jr.
Phone: 315 330-3145

This research was supported by the Defense Advanced Research Projects Agency of the Department of Defense and was monitored by Raymond P. Urtz, Jr. RADC (OCSE), GAFB, NY 13441 under Contract F30602-72-C-0470.

✓

PUBLICATION REVIEW

This technical report has been reviewed and is approved.

Raymond P. Utz Jr.

RADC Project Engineer

Summary

The investigations on this program have included the measurement of multiwavelength scintillation statistics over a very long, highly turbulent path; the analytical and experimental study of finite-transmitter and wander-tracking effects on target irradiance; and the study of the detailed nature of microthermal turbulence fluctuations, including turbulent intermittency, as related to short-term scintillation statistics. The latter two areas represent ongoing efforts, and are reviewed in this report.

Finite-beam experiments are being conducted with a wander-cancelling, tracking-transmitter over a 1.6 km, uniform path. A new prediction is given for the transverse amplitude correlation length under near field conditions in strong turbulence. A useful, physically derived approximation to combined diffraction, wander, and short-term beamspread angles or mean target irradiance is presented, and shown to agree well with more rigorous numerical calculations; experiments under strong turbulence conditions show a substantial and surprising advantage for wander-tracking. The normalized variance of the fluctuating irradiance (strength of fading) due to scintillation, wander, and coherent fading is also discussed, and probability distributions and spectra of wander and irradiance are presented.

Microthermal fluctuations due to turbulence are considered, and it is shown experimentally that the statistics of appropriately averaged first-increments or derivatives behave in accordance with recent theoretical predictions. Short-term turbulence and scintillation statistics are discussed, including intermittency effects. It is pointed out that the level-crossing and conditional probability problems for the scintillating irradiance are complicated by the non-Markovian nature of this process.

Table of Contents

I. Introduction

Work on this program has been concerned with three remaining aspects of turbulence-induced scintillations which have been poorly understood:

1) Scintillation effects far into the multiple scattering or "saturation" regime.
2) The effects of beam-wave or finite-aperture transmitters, including the influence of combined wander, scintillation, and short-term spread on target irradiance. This includes the advantages and parameter-dependencies of wander-cancellation through tracking.
3) The nature and effects of the intermittency of turbulence on scintillations.

The results and status of these respective efforts will be reviewed in the following sections. The latter two topics represent ongoing investigations for a follow-on program, and the emphasis in the present report will be on investigations conducted during the final quarter of the contract period. The reader is referred to preceding Quarterly Progress Reports for details of the preceding efforts.

II. Long-Path Scintillations

Scintillation statistics were measured at 4880 Å and 10.6 μ wavelengths over a very long, low path, in order to experience very high integrated-path turbulence. The pathlength L was 6 km. The results are presented in an earlier report[1] and recent paper;[2] these include the observation of saturation of scintillations at 10.6 μ, and heretofore unobserved anomalies in the behavior of covariance functions and scintillation spectra. We briefly discuss here some recent additions to the understanding of this regime.

In addition to Brown's numerical analysis[3] for a two-dimensional case, there now exist two highly physical treatments of multiple scattering or scintillation in strong turbulence.[4,5] These treatments are generally similar, although the results disagree as to the behavior of the log amplitude variance with increasing pathlength or turbulence "beyond saturation".[6]

Significantly, both treatments predict the profound change in covariance behavior which was observed in the long-path experiments.[1,2] As the first-order or Rytov theoretical log amplitude variance (σ_T^2) increases,[6] the covariance is predicted to drop rapidly and develop a long tail, such that two (i.e., small and large) transverse amplitude correlation scales emerge in place of the familiar $(\lambda L)^{1/2}$. The large correlation scale implies poor receiver aperture averaging of scintillations, while the short scale implies the existence of surprisingly high scintillation frequencies (several kHz at visible wavelengths); both of these phenomena are observed.

The latter effect is of especial importance, since scintillation experimenters have long assumed that one kilohertz represents an adequate frequency response for measurement apparatus, and that the necessary condition for "point" performance of a small receiver was that its diameter be smaller than $(\lambda L)^{1/2}$. It is now clear that these are not sufficient conditions, and that further experiments are desirable.

Although our 10.6 μ results were not affected, the interesting regime of $\sigma_T^2 >> 1$ should be further investigated at shorter wavelengths. For example, the behavior of experimental log amplitude variance (σ_E^2) vs σ_T^2 is cast in doubt; although we suspect that the negative slope or "supersaturation" is a fact, the actual slope and existence of an asymptote are not verified.

Yura has extended his analysis to explicitly predict scintillation spectra in this regime.[7] We have just received this work as of this writing, and we will compare these predictions with our data below 1 kHz. It is clear that the general features are in agreement. We are also considering the possibility of correcting those σ_E^2 values which are affected by spatial and electronic filtering. However, Yura's results are for a plane wave source and omit certain coefficients; it would be far preferable to conduct new experiments over our long-path facility using very small receivers and large measurement bandwidths.

III. Finite-Beam Effects

As described in the preceding report, the equipment which has been fabricated for measuring finite-beam effects (including tracking-out of atmospherically induced wander) has been installed at our regular field site, which is flat and uniform and includes micrometeorological instrumentation. The tracking transmitter is mounted on a massive concrete slab which is isolated from the transmitter shack. Wander-tracking and target-irradiance signals are recorded for digital processing. During the recent period, certain minor improvements were completed and the facility is now under full operation for a program of quantitative experiments at 6328 Å. High-turbulence results are being obtained during the summer, and lower-turbulence data--which will scale to the 10.6 μ case--will be conducted through the coming months.

Efforts are continuing on the clarification and unification of the theory using the approach first reported in Ref. 1. In the present report, further theoretical considerations are discussed, and preliminary, representative experimental results are given.

A. Amplitude Correlation Scale (Scintillation Patch Size)

The nominal size of the transverse amplitude correlation length (ρ_a) has been a matter of considerable confusion. We believe that it is now possible to confidently predict this parameter under a variety of conditions, as follows.

We confine ourselves to a statistically homogeneous (horizontal) path, and denote the following parameters:

Optical/infrared wavenumber	k
Turbulence strength[6]	C_n^2
Pathlength	L
Coherence scale[6]	$\rho_o \sim (k^2 L C_n^2)^{-3/5}$
Transmitter diameter	b
Rytov log amplitude variance	$\sigma_T^2 \sim C_n^2 L^{11/6} k^{7/6}$
Beamwidth at receiver	w ($\geq \rho_a$)

In all near-field ($b > \sqrt{\frac{L}{k}}$) conditions, the transmitter is assumed to be focused. We omit coefficients of order unity, and hence we do not distinguish between ρ_o for plane and spherical wave sources.

Considering scintillations only, i.e. omitting beam wander effects, the amplitude correlation scale values are given in Table I. For comparison, the nominal beam sizes are also given (Ref. 1).

Table I

Amplitude Correlation Scale (ρ_a) and Beamwidth (w) at Receiver Plane

	$\sqrt{\frac{L}{k}} < \rho_o$ (i.e. $\sigma_T^2 < 1$)	$\sqrt{\frac{L}{k}} > \rho_o$ (i.e. $\sigma_T^2 > 1$)
$b < \sqrt{\frac{L}{k}}, \rho_o$	a) $\rho_a = \sqrt{\frac{L}{k}}$, $w = \frac{L}{kb}$	d) $\rho_a = \rho_o$, $w = \frac{L}{kb}$
$\sqrt{\frac{L}{k}} < b < \rho_o$	b) $\rho_a = \frac{L}{kb}$, $w = \frac{L}{kb}$	
$\sqrt{\frac{L}{k}} > b > \rho_o$		e) $\rho_a = \rho_o$, $w = \frac{L}{k\rho_o}$
$b > \sqrt{\frac{L}{k}}, \rho_o$	c) $\rho_a = \frac{L}{kb}$, $w = \frac{L}{k\rho_o}$	f) $\rho_a = \rho_o^2/b$ $(< \rho_o)$, $w = \frac{L}{k\rho_o}$

Discussion

Condition (a) corresponds to a far-field source with first-order theory applicable.[6]

Case (b) is for a near-field source with first-order theory applicable, and is the only condition for which the patch and total beam sizes are nominally the same. This represents the "transmitter smoothing of scintillations" predicted by the first-order theory and illustrated by the photograph of Fig. 1 of Ref. 9: there is a relatively stable central spot, with little scintillation around it.

Condition (c) represents the interesting case in which the first-order theory breaks down for a finite transmitter ($b > \rho_o$) even though it is valid for a plane or spherical wave source ($\sigma_T^2 < 1$). This is the realm predicted in Ref. 9 and illustrated by the photograph of Fig. 3 in that paper, which shows the proliferation of diffraction-scale patches. It has also been predicted by Goshelashvily.[10]

Conditions (d-f) are not describable by first-order theory. There is every physical and dimensional reason to believe that the results of Yura's analysis for a plane wave (Ref. 4), i.e. that ρ_a becomes ρ_o for $\sigma_T^2 > 1$, will also apply to a far-field source. The result given for condition (f), for a focused, large source, is derived from simple asymptotic (or breakpoint) consistency with cases (c) and (e). This is a novel result, and says that the effect of a large, focused transmitter aperture (b) in a strong, multiple-scattering regime is to yield a scintillation patch size = $\rho_o \times (\rho_o / b)(<< \rho_o)$. This physically corresponds to further breakup of ρ_o-sized patches into extremely small spots. It is to be hoped that Yura's analysis can be extended to cover such a condition, which realistically applies for a typical near-field (focused) condition with visible wavelengths and strong turbulence.

A particularly interesting behavior may be illustrated as follows. Suppose that we have a near-field transmitter and wish to determine the behavior of ρ_a as turbulence increases. We will then progress from case (b) to (c) and then (f), as shown in Table IA:

Table IA

Amplitude Correlation Scale (ρ_a) for Near-Field Transmitter and Increasing Turbulence

Condition	ρ_a
$\sqrt{\frac{L}{k}} < b < \rho_o$	$\frac{L}{kb}$
$\sqrt{\frac{L}{k}} < \rho_o < b$	$\frac{L}{kb}$
$\rho_o < \sqrt{\frac{L}{k}} < b$	ρ_o^2/b

This predicts that the patch size will remain that of the transmitter diffraction scale until ρ_o decreases to $(L/k)^{1/2}$ (i.e. $\sigma_T^2 \approx 1$), and then it will decrease as ρ_o^2/b as turbulence strength increases.

In all cases, the scintillation spectra will have a bandwidth $\sim v_n/\rho_a$, where v_n is the transverse wind velocity. Case (f) therefore implies very high scintillation frequencies ($\gtrsim$ 10 kHz)--enhanced by a factor of b/ρ_o compared to those observed in Ref. 1 and predicted in Ref. 7.

We remark here that this predicted phenomenon of an even greater degree of breakup, for strong and increasing turbulence and a focused, near-field transmitter, may be manifested by an increase in log amplitude variance or total scintillation level over that naively expected; that is, the final asymptotic behavior in Figure 20 in Ref. 1, which is the log amplitude variance for large b, may be larger or more complicated than expected. Of course, the high frequencies and small patch sizes involved make accurate scintillation measurements difficult and in many cases may indicate diminishing practical importance in target illumination situations.

Finally, we note that the ultimate breakdown of turbulence MTF

theory (and e.g. the existing expressions for ρ_o) for strong turbulence scattering is not known. Nevertheless, the present expressions for ρ_a represent a significant--and probably sufficient--extension from the first-order scintillation theory.

Experiments

The ρ_a predictions for cases (d-f) in Table I may be verified through photographs of the scintillation patches at the receiver plane, as was done for cases (b) and (c) in Ref. 9. This will be undertaken if sufficiently straightforward with existing facilities. Ultimately, it would be highly desirable to employ large-bandwidth electronics with very small receivers, to accurately measure covariance and variance effects in this regime. Case (d) then represents the situation of Sec. II, and case (f) a large-aperture extension of it. Note, however, that a very long path is not required for case (f).

B. Finite-Beam and Tracking Effects on Mean Target Irradiance

In this section, we extend the description begun in Ref. 1 of finite-transmitter and wander-tracking effects on the first moment of target irradiance (average illumination) on the long-term beam axis. The approach, which utilizes recent developments in Huygens-Fresnel theory[11,12] and reciprocity,[11-13] involves the simple mean-square addition of the individual angular beamspread mechanisms, and resolves contradictions and inconsistencies in the literature.[1] As will be seen, the expressions represent an excellent approximation to more rigorous numerical results, while retaining clear physical meaning and dimensional consistency. The discussion will also point out theoretical work which remains to be completed. The present discussion will be confined to the case of a negligible inner scale of turbulence; the extension to non zero ℓ_o is indicated in Ref. 1.

We first point out that integral expressions for the long-term (no wander-tracking) and short-term (wander-tracked) mean irradiance are given in Ref. 14, and that these expressions can be numerically evaluated for an arbitrary transmitter wave. An exact analytical solution is probably not possible, which indicates that the approximate solution given below in

terms of separate physical mechanisms, simply fails to take into account some degree of "coupling" between these mechanisms. Numerical results for a gaussian beam may be readily obtained and would be quite useful. Related numerical results for a uniformly illuminated lens have been given by Kon,[15] and, through reciprocity, by Fried.[16,17] The latter will be discussed further below and related to the present approximate analysis.

1. Calculation of Spread Angle from Physical Beamspread Mechanisms

The separate beamspreading or irradiance-reducing mechanisms are readily derived to within a numerical constant. We initially defer the specification of these constants, which avoids the specification of the transmitter beam wave (gaussian, truncated gaussian, uniform circular, etc.), thus preserving generality. Also, it avoids the question of competing angular definitions such as 1/e diameter, second spatial moment, etc., which can yield significantly different results.[18,19] It is implicit in our development that angular spreads are defined in terms of on-axis irradiance, which is the important quantity.

We now write the expressions for each respective beam-spreading mechanism as follows:

Diffraction Angle

$$\text{Mean-Square Diffraction Angle} \sim \frac{1}{(kb)^2} \qquad (1a)$$

where k is the optical/infrared wavenumber, and b the transmitter beam diameter by an appropriate measure.

Geometric Angle

$$\text{Mean-Square Geometric Spread Angle} \sim b^2 \left(\frac{1}{L} - \frac{1}{R} \right)^2 \qquad (1b)$$

where L is the transmitter-target distance and R is the transmitted wavefront curvature. In particular, this term is zero for the focused case ($R=L$).

Wander Angle

We obtain the wander angle by applying the reciprocity principle to receiver image dancing (Ref. 1):

$$\text{Mean-Square Wander Angle} \sim \frac{D_\phi(b)}{k^2 b^2} \sim (b/\rho_o)^{5/3} \frac{1}{k^2 b^2}$$

$$= (\rho_o/b)^{1/3} \frac{1}{k^2 \rho_o^2} \qquad (1c)$$

where D_ϕ is the phase structure function,[6] and ρ_o is the coherence scale, as observed at the receiver, for a conceptual point source at the target.[11-13]

It may easily be shown that this is a geometrical-optics expression, which does not actually involve k. However, the final form shown is convenient for comparison with other terms.

Atmospheric Beam Spread

Finally, we consider the short-term atmospheric beam spread. This has previously[1,11,12] been given in the asymptotic form for $b >> \rho_o$, as $(1/k^2\rho_o^2)$; this is the regime of "beam break-up". However, the details of this mechanism for b comparable to ρ_o can be important, especially if wander is cancelled out, and we write

$$\text{Mean-Square (Short-Term) Spread Angle} \sim f(b/\rho_o) \frac{1}{k^2 \rho_o^2} \qquad (1d)$$

where $f(b/\rho_o)$ can be obtained from a complete (numerical) analysis and will be discussed later. Note that $f(\frac{b}{\rho_o} \to \infty) = 1$.

Total Angular Spread

We now assume a focused condition, and write the total mean-square angle Φ^2 from Eqs. (1a-1d) as

$$\Phi^2 = (\text{diffraction}) + (\text{wander}) + (\text{short-term spread})$$

$$= \frac{C_1}{k^2 b^2} + \left[C_2 \left(\frac{b}{\rho_o}\right)^{-1/3} + C_3 \, f\left(\frac{b}{\rho_o}\right) \right] \frac{1}{k^2 \rho_o^2} \qquad (2)$$

In the event that wander is tracked out, $C_2 = 0$.

For the case of fixed ρ_o and fixed transmitter size b, respectively, Eq. (2) can be usefully written as

$$\Phi^2 k^2 \rho_o^2 = \frac{C_1}{(b/\rho_o)^2} + \left[C_2 \left(\frac{b}{\rho_o}\right)^{-1/3} + C_3 \, f\left(\frac{b}{\rho_o}\right) \right] \tag{2a}$$

$$\Phi^2 k^2 b^2 = C_1 + \left[C_2 \left(\frac{b}{\rho_o}\right)^{-1/3} + C_3 \, f\left(\frac{b}{\rho_o}\right) \right] \frac{b^2}{\rho_o^2} \tag{2b}$$

Asymptotic log plots of these expressions are given in Figs. 1a, b. In Fig. 1a, increased abscissa corresponds to increased transmitter size, while in Fig. 1b, it corresponds to decreasing ρ_o or increasing turbulence strength and/or pathlength. The short-term spread function $f(b/\rho_o)$ cannot usefully be broken down into asymptotic linear segments, and is shown qualitatively in Figs. 1a, b.

Finally, with the determination of C_{1-3} in Eq. (2), the complete, continuous curves of Φ^2 will be specified. The conceptual curves with and without wander tracking are shown in Figs. 1a, b.

2. Angular Parameter α

As discussed below in conjunction with the second moment of irradiance, a parameter of importance is the ratio of mean-square wander to total short-term spread. From Eq. (2), this is given by

$$\alpha = \frac{C_2 \, \rho_o^{-5/3} \, b^{-1/3}}{\frac{C_1}{b^2} + C_3 \, f\left(\frac{b}{\rho_o}\right) \frac{1}{\rho_o^2}} \tag{3}$$

For a small aperture ($b \ll \rho_o$), diffraction predominates and we have

$$\alpha \sim \frac{b^{5/3}}{\rho_o^{5/3}} \sim D(b) \quad , \tag{4a}$$

where D is the wave structure function. For a large aperture ($b \gg \rho_o$), we

$$\alpha \sim \left(\frac{\rho_o}{b}\right)^{1/3} \quad . \tag{4b}$$

3. Corresponding First Moment or Mean Irradiance

The mean target irradiance at the long-term beam centroid is simply proportional to the reciprocal of Φ^2. Hence,

$$\bar{I} = I_o \frac{b^2}{\Phi^2 L^2}$$

$$= I_o \frac{b^2}{L^2} \frac{1}{\frac{C_1}{k^2 b^2} + \left[C_2 \left(\frac{b}{\rho_o} \right)^{-1/3} + C_3 f\left(\frac{b}{\rho_o} \right) \right] \frac{1}{k^2 \rho_o^2}} \qquad (5a)$$

where I_o is a measure of the irradiance at the transmitter. For reference in later discussion below, we also write this as

$$\bar{I} = I_o \frac{k^2 b^2}{L^2} \frac{1}{\frac{C_1}{b^2} + \left[C_2 \left(\frac{b}{\rho_o} \right)^{1/3} + C_3 f\left(\frac{b}{\rho_o} \right) \right] \frac{1}{\rho_o^2}} \qquad (5b)$$

4. Comparison with Numerical Results; Determination of Constants

For a given transmitter wavefront, the constants in Eq. (5a) might in some cases be determined from a more detailed consideration of the physical beamspread mechanisms. Alternatively, they may be determined through comparison with complete numerical solutions. Such a solution is available from the analysis of an optical heterodyne receiver;[17] through the principle of reciprocity,[13] this signal has a one-to-one correspondence with the target irradiance for a uniformly illuminated, focused, transmitting aperture.

The heterodyne analysis includes results with and without wavefront tilt-tracking, which correspond respectively to the cases of wander-tracking and a static transmitter. In particular, the maximum improvement in mean irradiance to be obtained through proper control of aperture size (b) and the employment of wander-tracking ($C_2 = 0$) can be predicted.

We first note that, in Eq. (5a), we have one redundant constant. We rewrite the expression as

$$\frac{\bar{I}}{I_\infty} = \frac{1}{\frac{C_1' \rho_o^2}{b^2} + \left[C_2' \left(\frac{b}{\rho_o} \right)^{-1/3} + f\left(\frac{b}{\rho_o} \right) \right]} \quad , \qquad (6)$$

where I_∞ is the asymptotic target irradiance for large b, and depends on $k^2 \rho_o^2$ (see Eq. 2a). We then note that the intersection of the diffraction and large-b, short-term beam spread asymptotes (Fig. 1) occurs in the heterodyne analysis at $b = r_o = 2.0986\, \rho_o$*. Hence we have

$$\frac{C_1' \rho_o^2}{(2.0986\, \rho_o)^2} = f\left(\frac{b}{\rho_o} \to \infty \right) = 1 \quad ,$$

$$\text{or} \quad C_1' = 4.40 \qquad (7)$$

for a uniformly illuminated transmitter.

To determine the detailed function $f(b/\rho_o)$, we use the heterodyne results for the tracking case ($C_2' = 0$). Identifying $\bar{I}/I_\infty$ with "antenna gain G" as defined in Ref. 17, we write from the reciprocal of Eq. (6):

$$\frac{1}{G} - \frac{4.40}{b^2/\rho_o^2} = f\left(\frac{b}{\rho_o} \right) \quad . \qquad (8)$$

The curve $f(b/\rho_o)$ as obtained from the numerical results of Refs. 16 and 17 is given in Fig. 2. For each value of the abscissa, the function f may be interpreted as the coefficient on the short-term, atmospherically induced beam spread relative to the large-aperture value $(1/k^2 \rho_o^2)$.

---

*Note that this number was incorrectly given as 2.15 in Ref. 1. Also, the appropriate ρ_o for the present case is the spherical wave value.[1]

For $b/\rho_o \lesssim 3$, the physical interpretation of this function is less simple since it increases for decreasing b, while the wavefront distortion and associated spreading (with linear tilt removed) should approach zero. This occurs because f in Eq. (8) becomes the small difference between two large numbers; in fact, this function actually manifests the "coupling" between diffraction by b and ρ_o. As $\frac{b}{\rho_o}$ further decreases, f has a negligible effect on G.

For large b/ρ_o, f is seen to approach unity surprisingly slowly. This regime will be discussed further in Section III-5.

Now that C_1' and f have been determined, we may choose C_2' such that Eq. (6) will best approximate the numerical results for the no-tracking case. An approximate optimum value is

$$C_2' = 1.80 \quad , \tag{9}$$

which establishes the relative weighting of the beam-wander effects on mean irradiance for this transmitter configuration.

The usefulness of the present approximation, i.e. using explicit physical mechanisms, can be tested by comparing the curve of Eq. (6) with the numerical results of Refs. 16 and 17 for the no-tracking case. This comparison is shown in Figure 3, where the tracking case ($C_2'=0$) is also shown for completeness. The approximation is seen to be quite good, which indicates that wander is largely independent or uncoupled from the other mechanisms. The relationship between these curves and the (reciprocal) asymptotic curves of Fig. 1a is readily apparent.

The case corresponding to Fig. 1b, i.e. with fixed b and variable ρ_o, can also be plotted using the same constants C_1' and C_2' and function $f(b/\rho_o)$. The ordinate must then be renormalized by multiplying the denominators of Eq. (6) by b^2/ρ_o^2 (see Eq. 2b); the normalizing quantity or asymptote at small b/ρ_o then corresponds to the irradiance for weak turbulence, which is determined by transmitter (free-space) diffraction and depends on k^2b^2.

5. Concept of Short-Term Coherence Scale ($\rho_{o_{st}}$) and Related Approximations

In a recent paper,[14] Yura discusses a "short-term" atmospheric mutual coherence function (MCF) in which linear wavefront tilt (or wander) has been removed.[16] The expression for this MCF is

$$M_{st}(\rho) = \exp\left\{-\left(\frac{\rho}{\rho_o}\right)^{5/3}\left[1-0.62\left(\frac{\rho}{b}\right)^{1/3}\right]\right\} \tag{10}$$

where ρ_o is the coherence scale used in the preceding expressions, and represents the 1/e point of the conventional or "long-term" MCF. Yura then similarly defines a "short-term" coherence scale, $\rho_{o_{st}}$, as the 1/e point of $M_{st}(\rho)$; it may be noted that $\rho_{o_{st}}$ is a function of the (uniformly illuminated) transmitter aperture size b. The purpose of the present discussion is to show that certain approximations are incorrectly applied in Ref. 14, and that, contrary to that development, the physical utility of $\rho_{o_{st}}$ is marginal at best. Hence that paper does not properly treat the problem of wander cancellation and beam spread.

From Eq. (10), we determine the value of $\frac{\rho_{o_{st}}}{\rho_o}$ as a function of b/ρ_o as follows. From the definition of $\rho_{o_{st}}$, we have

$$\left(\frac{\rho_{o_{st}}}{\rho_o}\right)^{5/3}\left[1-0.62\left(\frac{\rho_{o_{st}}}{b}\right)^{1/3}\right] = 1$$

or

$$\left(\frac{\rho_{o_{st}}}{\rho_o}\right)^{5/3} - 0.62\left(\frac{\rho_{o_{st}}}{\rho_o}\right)^{2}\left(\frac{b}{\rho_o}\right)^{-1/3} = 1 \tag{11}$$

The solution of this equation is plotted in Figure 4. It should be noted that, for $(b/\rho_o) < 1.21$, $\rho_{o_{st}}$ does not exist; i.e., M_{st} does not have a 1/e point.

In Ref. 14, the author approximates the solution of Eq. (11) by

$$\frac{\rho_{o_{st}}}{\rho_o} = 1 + 0.37\left(\frac{b}{\rho_o}\right)^{-1/3} \quad . \tag{12}$$

This is also plotted in Figure 4, from which it can be seen that the approximation is poor for $b/\rho_o \lesssim 10$. Unfortunately, in Ref. 14 the approximation is utilized extensively for $1.0 \leq b/\rho_o \leq \infty$, and in particular in the regime below 10. (Note: the author's abscissa is the reciprocal of that used here). Therefore, Figs. 2-4 in that reference are without value and, in fact, $\rho_{o_{st}}$ does not even exist for $\rho_o/b > 0.83$.

A related difficulty with Ref. 14 is that the author equates the short-term (or wander-removed) atmospheric beam spread to $1/k^2\rho_{o_{st}}^2$, which is equivalent to identifying the function f of Eq. (1d) and Fig. 2 with $\rho_o^2/\rho_{o_{st}}^2$. However, there is no physical basis for this use of $\rho_{o_{st}}$ except for $b \gg \rho_{o_{st}}$, in which case $\rho_{o_{st}} \approx \rho_o$ and $\rho_{o_{st}}$ becomes trivial. Similarly, he equates the long-term (including wander) beam spread to $1/k^2\rho_o^2$, which is likewise incorrect except for $b \gg \rho_o$. Hence, even if the author had utilized the correct values of $\rho_{o_{st}}$, the interpretations in terms of angular spread or mean irradiance would be erroneous.

In order to gain further insight into this problem, we may define a $\rho_{o_{eff}}$ such that atmospherically induced beam spread is given by $1/k^2\rho_{o_{eff}}^2$ for any value of b/ρ_o. From Eq. (2):

$$\frac{1}{k^2\rho_{o_{eff}}^2} = \frac{1}{k^2\rho_o^2}\left[C\left(\frac{b}{\rho_o}\right)^{-1/3} + f\left(\frac{b}{\rho_o}\right)\right] \tag{13}$$

where $C = C_2/C_3 = 1.80$ in the long term case discussed previously, and $C = 0$ in the short term or wander-tracked case. In the long term case, $\rho_{o_{eff}}$ is approximated by ρ_o only for b/ρ_o large enough that wander is negligible and f converges to unity. For the short term case, $\rho_{o_{eff}}$ is approximated by $\rho_{o_{st}}$ only for b/ρ_o large enough that f converges to $(\rho_o^2/\rho_{o_{st}}^2)$.

Finally, we note from Eq. (12) that

$$\left(\frac{\rho_o^2}{\rho_{o_{st}}^2}, f \right) = 1 - 0.74 \left(\frac{b}{\rho_o} \right)^{-1/3} \qquad (14)$$

$$\frac{b}{\rho_o} \gg\gg 1$$

The approach to unity is thus very slow, due to the -1/3 exponent; it is within one percent for $b/\rho_o \geq 4 \times 10^5$. Hence the convergences in the preceding paragraph occur very slowly.

6. Use of Approximate MCF's

The basic Huygens-Fresnel integral expression for mean irradiance[14] has been solved analytically for a gaussian beam by Titterton,[20] using an approximate MCF in which the 5/3 exponent on (ρ/ρ_o) is replaced by 2. This has been shown to be equivalent to eliminating all wavefront distortion terms except linear tilt.[21] Unfortunately, this seemingly minor approximation in the exponent leads to results which are dimensionally inconsistent and therefore misleading. However, the approach is worthy of discussion.

Specifically, the result corresponding to Eq. (5b) is

$$\bar{I} = I_o \frac{k^2 b^2}{L^2} \frac{1}{\frac{1}{b^2} + \frac{2}{\rho_o^2}} \qquad (15)$$

$$\sim \frac{1}{1 + 2\frac{b^2}{\rho_o^2}} \qquad (15a)$$

An earlier analysis of wander alone[22] gives the result

$$\bar{I} \sim \frac{1}{1 + 2a} \quad , \qquad (16)$$

where a is the ratio of mean-square wander to instantaneous beam width. By comparing Eqs. (15) and (16), it is tempting to identify a with b^2/ρ_o^2,

and to identify the two denominator terms of Eq. (15) as diffraction and wander, respectively. However, wander is in fact a geometrical-optics phenomenon, and comparison with Eq. (5b) shows that the final term in Eq. (15) is dimensionally related to atmospherically induced beam spread rather than wander. The dimensionally correct expressions for a are given in Eqs. (3,4).

Similarly, direct calculations of wander from the definition of Ref. 23, or from the phase structure function and reciprocity as applied to wavefront tilt,[20] lead to the same, incorrect results when the approximate MCF is employed.

This approximate MCF approach will be discussed further in connection with the second moment in a subsequent section.

C. Finite-Beam and Tracking Effects on Irradiance Fading or Second Moment

1. Analysis of Fading

As discussed in Ref. 1, the physics of fading may be separated into the following three mechanisms:

a) Wander-fading

b) Scintillation (first-order)

c) Beam-breakup or coherent fading.

The statistics of wander fading are predicted to be beta-distributed,[22,24] while the latter two mechanisms are thought to be log normal. To determine the total fading, the individual variances are added.

Wander Fading

Utilizing results from Esposito,[25] Titterton has shown[22] that the normalized variance of irradiance due to wander is given by

$$\sigma^2_{I_{\text{wander}}} = \frac{4a^2}{4a+1} \tag{17}$$

where a has been defined previously and is correctly given by Eq. (3).

Scintillation

First order scintillation for a finite transmitter has been solved by several investigators.[6] Detailed numerical results for the log amplitude variance are given by Kerr and Eiss.[26] In the present context, where we are unfortunately forced to deal with the linear irradiance rather than the more meaningful log quantities, it is customary to write[27]

$$\sigma^2_{I_{\text{scintillation}}} = e^{4\beta\sigma^2} - 1 \quad . \tag{18}$$

In this expression, σ^2 is the log amplitude variance for a point transmitter, and β represents a "transmitter aperture smoothing" term which is related to the reciprocal, receiver-aperture smoothing in a heterodyne receiver. In order to write Eq. (18), the scintillations must be assumed to be log normal. Providing that the transmitter wavefront is carefully adjusted,[9] the value of β can decrease significantly as the aperture is increased.[26] Rather than relate β to the approximate analysis of direct-detection receivers in the literature, as is customary,[16] we may precisely define β by specifying that the log amplitude variance results in Ref. 26 are equal to $(\beta\sigma^2)$.

Beam Breakup or Coherent Fading

As the transmitter aperture b becomes greater than ρ_o, the beam at the target breaks up, i.e., it shows substantial short-term spread. This is accompanied by an increase in fading with increased aperture size which is not predicted by first-order scintillation theory, and which is related to the reciprocal case of "coherent fading" in an optical heterodyne receiver.[27] The effect is presumably an added mechanism for log normal scintillations. Unfortunately, this situation has not been well analyzed; relevant work includes the approximate coherent fading analysis of Ref. 27, and the finite-transmitter, multiple-scattering analysis of Ref. 10. The latter purports to directly show the breakdown of first-order theory for $b \gtrsim \rho_o$.

For an arbitrarily large transmitter, the results of Ref. 27 imply that fading will increase without limit. However, this is not experimentally observed.[9] Rather, for the large, focused-transmitter case, we expect an

asymptote on the order of the plane wave variance. As discussed above in Sec. III-A, the situation may be especially complicated when the Rytov $\sigma^2_T >> 1$.

Brown[28] has given insight into the large-aperture problem by assuming a set of N mutually incoherent radiators on the aperture ($N = b^2/\rho_o^2 >> 1$), and showing that the normalized variance is

$$\sigma^2_{I_{\substack{\text{large aperture}\\ \text{coherent fading}}}} = 1 - \frac{1 - \left(e^{4\sigma^2} - 1\right)}{b^2/\rho_o^2} \qquad (19)$$

where the quantity in parentheses is the irradiance variance for a spherical wave source (Eq. 18). This shows that the asymptote is unity, which is reached at smaller b/ρ_o when σ^2 is large.

In general, we must admit that the coherent fading regime is poorly understood, and we therefore represent this term by

$$\sigma^2_{I_{\text{coherent fading}}} = g \quad , \qquad (20)$$

where g is a function whose general--but not detailed--behavior is known.

Combined Fading

If we now assume the independence of the fading mechanisms, we write from Eqs. (17, 18, and 20):

$$\sigma^2_{I_{\text{total}}} = \frac{4\alpha^2}{4\alpha+1} + \left(e^{4\beta\sigma^2} - 1\right) + g \quad . \qquad (21)$$

The proper independent variable for α is (b/ρ_o), as can be seen from Eq. (3) by multiplying the denominator and numerator by b^2. The first-order scintillation term depends on σ^2 and $b/\sqrt{L/k}$, and we note that σ^2 is related to ρ_o by

$$\sigma^2 = 0.228 \left[\frac{\sqrt{L/k}}{\rho_o}\right]^{5/3} \qquad (22)$$

The g-dependence is unknown but probably depends primarily on (b/ρ_o), and secondarily on σ^2 and perhaps $\sqrt{L/k}$. Hence, a single, universal curve cannot be drawn.

The asymptotic behavior of the wander-fading term vs (b/ρ_o) is obtained from Eqs. (3) and (17), and is discussed in Ref. 1. For the wander-tracked case, α is taken as zero.

The general behavior of $\sigma_{I_{\text{total}}}^2$ vs b is shown in Fig. 5a for fixed ρ_o, $\sqrt{L/k}$, and σ^2. To derive a similar curve for variable ρ_o^{-1} and fixed b and $\sqrt{L/k}$ (and hence fixed β), we use Eq. (22) to write the first-order scintillation term as

$$e^{4\beta\sigma^2} - 1 = \exp\left\{0.912\ \beta\left[\frac{\sqrt{L/k}}{\rho_o}\right]^{5/3}\right\} - 1$$

$$\approx 0.912\ \beta\left[\frac{\sqrt{L/k}}{\rho_o}\right]^{5/3}, \qquad (23)$$

where we assume $\beta \ll 1$. The resultant curve is shown in Fig. 5b.

2. Comparison with Approximate Analyses

Using the Huygens-Fresnel approach, the approximate MCF discussed in a previous section, and certain other approximations, Titterton has derived the following expression for the normalized variance:[20]

$$\sigma_I^2 = \frac{4\left(b^2/\rho_o^2\right)^2 e^{4\beta\sigma^2}}{4\frac{b^2}{\rho_o^2} + 1} + \left(e^{4\beta\sigma^2} - 1\right) \qquad (24)$$

It is interesting to compare this result with Eq. (21); if we identify α with (b^2/ρ_o^2), we may identify the first term with wander-fading and the second with scintillation. There is no term for coherent fading, and a cross-coupling of wander-fading and scintillation has apparently arisen. However, as discussed previously, this identification of α is clearly inconsistent. Some of

the same approximations were also employed in Ref. 27. It is obviously very desirable to obtain a (probably numerical) result which is free of these approximations.

D. Representative Experimental Data

1. Introduction

In this section we present some preliminary, representative data on finite-beam and wander-tracking effects. These data were taken under high turbulence conditions, such that $b >> \rho_o$. Extensive additional data will be collected under a variety of conditions.

A summary of the data being collected appears in Table II, and the experimental and data processing parameters are given in Table III.

Table II. Experimental Data Collected for Finite-Beam and Wander-Tracking Effects

Tracker (transmitter) end:	Real-time wander signal (servo-drive signal)
Target (receiver) end:	Real-time linear and log irradiance signal
	Mean irradiance
	Strength of turbulence (C_n^2, ρ_o)
	Real-time microthermal fluctuations
	Meteorological parameters

Table III. Experimental and Data Processing Parameters

Transmitter and beacon wavelengths: 6328 Å

Transmitter power: 75 mW

Path: 1.6 km, flat farm land

Beam height: 1.8 m

Mean-irradiance averaging time: 100 sec

Variance of log and linear irradiance and wander signal:

Digital computation with 10 sec averaging time,

300 sec data records

Irradiance and wander spectra: Digital computation with

0.1 Hz resolution, 100 sec averaging time; analog

computation with 1 Hz resolution, 100 sec averaging time

Irradiance probability distributions: digital computation

Digital sampling rate: 1 kHz

Target receiver bandwidth: 1 kHz

Target receiver aperture: 0.6 cm ($\sqrt{\frac{L}{k}}$ = 1.3 cm)

Target beacon aperture: 0.6 mm

Transmitter aperture: truncated gaussian beam, precisely focused, 15.2 cm

Inner scale determination: from spectrum of microthermal signal

---

The tracker servo resonance is at several hundred Hz, and the tracker closed-loop response, which is a function of gain settings and atmospheric conditions, is much faster than the beam wander effect.

The tracker system utilizes a quadrant photodetector and (x, y) galvanometric mirror scanners to maintain the target-beacon image coincident with the axis of the transmitter laser; hence, the instantaneous mean angle-of-arrival of the beacon wavefront at the transmitter aperture is matched by the outgoing transmitter wave. Since the beacon-image--and transmitted beam--are spread out by the atmosphere, the system actually operates on the centroid of the image distribution. It has been pointed out[29] that this centroid differs from the conventional first-moment definition, owing to the nature of the quadrant detector:

$$\text{Tracker "centroid" displacement} = \int i(x)\ \text{sgn}\ (x)\ dx \qquad (25)$$

where i(x) is the image irradiance distribution. However, it is physically apparent that the distinction is not critical, and this contention is supported by the detailed experimental results.

A much more important consideration is the following. In our application of reciprocity, in which we use a fast-tracking transmitter and

target to cancel beam wander, it is implicit that the entire transmitted beam is refracted uniformly by the atmosphere: that is, the image of the point-beacon must accurately indicate the tracking deflection necessary to cancel the wander or centroid displacement on the target. Under high turbulence conditions ($b >> \rho_o$), the beam is substantially broken up, and rays reaching the transmitter from the beacon may not accurately indicate the refraction of more than part of the beam.

This situation, which is similar to an isoplanatic patch argument, can result in inaccurate centering of the instantaneous, transmitted beam centroid on the target beacon. That is, the instantaneous centroid of the amorphous, broken-up beam may move around rapidly; in fact, the beam can then be envisioned in terms of separate bundles which wander independently.

This effect may be expected to average-out over relatively short periods (e.g., a fraction of a second), which is confirmed by visual observation at the target. Furthermore, the significant wander, even for a badly broken-up beam, tends to be surprisingly uniform over the beam, which indicates the prism-like effects of turbulence scales which are larger than those included in the theoretical (inertial subrange) model. The latter phenomenon accounts in part for the surprising improvement in target illumination which is observed with wander-tracking under conditions of strong turbulence, as discussed in a later section.

Perfect centering of the transmitted beam centroid on the desired target point can in principle be achieved with a sophisticated, image-processing tracking system which operates on the extended image of the finite, illuminated target area.

2. Wander Signal

RMS Wander Angle

The recording of the wander-tracking signal at the transmitter was begun just prior to the writing of this report. In the first such run, the results for the rms angular wander were (perhaps fortuitously) in good agreement with the theoretical prediction:

Measured C_n^2: $5.14 \times 10^{-14}\ m^{-2/3}$

Calculated ρ_o: 6.5 mm

Approximate effective aperture (b) = 15.2 cm

Approximate predicted rms wander angle =

$$\left(\frac{2\left(\frac{b}{\rho_o}\right)^{5/3}}{k^2 b^2} \right)^{1/2} = 13.0\ \mu\text{ rad}$$

Measured rms wander angle = 15.4 μ rad

Wander Spectrum

Theoretical predictions exist for the power spectral behavior of the optical phase difference between two points.[30,31,32] This may also be applied to the spectrum of image dancing or wander.[32] For the particular data run under discussion here, the wind velocity was very low, and the applicable prediction is

$$\text{Power spectrum of phase difference} \sim \omega^{-8/3} . \qquad (26)$$

The power spectrum and frequency-weighted power spectrum of the wander-tracking signal is shown in Fig. 6. The log-log slopes were very nearly equal to -8/3 and -5/3 respectively, which is consistent with the above prediction.

Wander Distribution

It is generally assumed that a one-dimensional component of beam wander is normally distributed.[22] The distribution of the vertical component of the wander signal for the data run under discussion here is shown in Figure 7. Marked asymmetry about the mean is noted, which is probably a manifestation of slow, large-scale, vertical refractive effects.

3. Target Signal

We now present representative results for the target irradiance with and without wander-tracking, from eight data runs in strong turbulence. These runs represent the condition ($b >> \rho_o$), and in some cases

may be affected by the inner scale, since ρ_o is small. Although the inner scale has been determined through microthermal spectra for each run, we have not yet attempted to modify the theoretical predictions for those cases. Although we are taking advantage of summer conditions for the high-turbulence data, the more interesting case of b comparable to ρ_o will be examined later; in particular, that is the case which scales to 10 micron systems.

Irradiance vs Time

The target irradiance on the beam axis is shown in Fig. 8a without wander-tracking and Fig. 8b with tracking. The irradiance is smoothed over a 1 second averaging time, in order to reduce the influence of scintillations. From these records, for which $b/\rho_o = 34.9$, the substantial advantage in mean irradiance and reduced fading to be obtained from tracking is qualitatively obvious.

Mean Irradiance

The mean irradiance on the beam axis, corrected for changes in transmitter power from run to run, is shown in Fig. 9. Since b is fixed and ρ_o is varied, this case corresponds to the reciprocal of Fig. 1b; we expect a minus two (log-log) slope at large b/ρ_o, although Fig. 2 demonstrates that the slope will still be distorted by $f(b/\rho_o)$ at $b/\rho_o \lesssim 300$. For variable ρ_o, we do not as yet have a detailed numerical prediction such as that of Fig. 3 for variable b.

The ratio of the mean irradiance for tracking vs no tracking is shown in Fig. 10. The theoretical prediction, which is a universal curve, is calculated from the results of Ref. 16 for a uniform transmitter aperture. It is seen that the improvement realized by tracking is generally significantly greater than that predicted for such large b/ρ_o; we surmise that this is due to beam refraction from turbulence scales which are larger than the outer scale and hence not included in the theory.

Fading

The log amplitude variance of the fluctuating target signal

is given for the wander-tracking and no-tracking cases in Table IV, as a function of measurement bandwidth. In the no-tracking case, the total fading consists of components due to beam-breakup scintillation (or coherent fading), and wander, while in the tracking case, the wander is removed. Since wander is a low-frequency phenomenon, the reduction in variance is seen to be most substantial when higher frequency (scintillation) components are either spatially or electronically filtered out.

The full-bandwidth (1 kHz) data of Table IV may be related to the curves of Fig. 5b by determining the normalized, linear irradiance variance (σ_I^2) instead of the log amplitude variance. The latter quantity is more indicative of dynamic range (the dynamic range of fading in dB $\approx$ 100 σ^2 for the log normal case[1]), but the limited theoretical treatments available for this regime tend to deal with σ_I^2. For the log normal case, which does not apply when wander-fading is substantial, the two variances are related by

$$\sigma_I^2 = e^{4\sigma^2} - 1 \tag{27a}$$

$$\sigma^2 = \frac{1}{4} \ln (\sigma_I^2 + 1) \tag{27b}$$

Rather than making use of these relationships, we will reprocess the data directly for σ_I^2. It may be noted that, according to Eq. (27a), σ_I^2 exceeds unity for the full-bandwidth data of Table IV.

Spectra of Fading

Typical power spectra for the log-amplitude with and without tracking are shown in Fig. 11, and the low-frequency contribution from wander is readily apparent. The frequency-weighted spectra will often show a double-peaked behavior for the no-tracking case, where the low and high frequency peaks correspond respectively to wander and scintillations.

Probability Distribution of Fading

The probability distribution of fading without tracking includes the combination of log normal scintillations and, theoretically, exponentially

Table IV. Log Amplitude Fading Variance vs Bandwidth, With (T) and Without (NT) Wander-Tracking

$\frac{b}{\rho_o}$	$\sigma^2_{1\text{ kHz}}$ NT	T	$\sigma^2_{10\text{ Hz}}$ NT	T	$\sigma^2_{1\text{ Hz}}$ NT	T	Ratio $\frac{\sigma^2_T}{\sigma^2_{NT}}$ 1 kHz	10 Hz	1 Hz
87.1	.307	.221	.130	.042	.033	6.10×10^{-3}	0.72	0.32	0.185
100.6	.268	.263	.088	.039	.022	5.44×10^{-3}	0.98	0.44	0.25
87.6	.460	.322	.156	.035	.019	3.87×10^{-3}	0.70	0.224	0.204
95.7	.300	.221	.083	.019	.019	2.49×10^{-3}	0.74	0.229	0.131
113.0	.353	.272	.112	.040	.030	4.60×10^{-3}	0.77	0.357	0.156
403.0	.290	.216	.107	.034	.027	4.36×10^{-3}	0.745	0.318	0.161
68.1	.330	.253	.066	.022	.014	3.007×10^{-3}	0.767	0.333	0.215
34.9	.432	.214	.238	.063	.032	0.011	0.50	0.265	0.344

distributed wander-fading. These distributions have not yet been measured in detail; the two fading mechanisms may be largely separated through spectral filtering, as discussed above.

Typical distributions of log amplitude are shown in Figure 13. As expected, the distribution becomes much more closely log normal when wander-tracking is employed.

IV. Short-Term Turbulence and Scintillation Statistics; Intermittency

A. Introduction

In this effort we are concerned with modeling the microthermal field in such a manner that short-term scintillation statistics can be predicted and related to turbulence statistics. The goal in this work is to understand measurement confidence intervals, conditional scintillation statistics, scintillation level crossings and deep fading, and ultimately phase and imaging effects, as related to finite or short measurement times and to the often observed sporadic (intermittent) nature of the turbulence mechanism.

In order to implement this study, we are utilizing the two-wavelength (4880Å and 10.6 μ) propagation facility and an array of microthermal sensors, the latter for spatial correlation measurements on the intermittent turbulence field. The raw data are magnetically recorded and then processed on a PDP-11 computer, which is programmed to perform a variety of functions:

Probability Computations

- Probability distribution of scintillation and single- or double-probe microthermal data
- First four moments and central moments
- Skewness, kurtosis

- Above quantities for absolute value of signal (with corrected mean)
- Above quantities for square of signal (or other function of signal)

- Above quantities with recursive, first-order digital (RC) filter, for signal or function of signal (variable averaging before computation of probability parameters)

Above quantities for first or second (finite-difference) derivatives of signal

Variance vs averaging time of signal or function of signal, and mean and variance of variances

Spectral Computations

FFT for spectra from 1 Hz to 500 Hz with 1 Hz resolution (averaged over many individual spectra taken over 1 sec each)

Low-frequency spectra from low-pass-filtered signal (lowest frequency limited by length of data record)

Frequency-weighted spectra

Log spectra.

The major goals of this investigation will be accomplished in a follow-on program. In this report, we will briefly indicate the types of data and analyses which are pertinent, and the theoretical issues involved.

B. Temperature Statistics

There has been a significant amount of theoretical work in the literature on the statistical properties of turbulent fields, including hypotheses on the forms of the distributions, the nature of the moments, and the effects of averaging. In our preliminary investigations, we have found better empirical agreement with certain of these theoretical treatments than has been heretofore reported. The details are described below.

Microthermal Fluctuations and Scintillations (Qualitative)

Typical single-probe fluctuations for strong-turbulence conditions and a low ($\lesssim$ 1 m/sec), unstable wind speed are shown in Fig. 14. Although this particular record does not represent conditions of pronounced intermittency, the sharply asymmetrical nature of the fluctuations is apparent. In Fig. 14b, a ramp-like structure may be discerned as described in the literature.[33] Similar fluctuations for a steady, 6 m/sec wind are shown in Fig. 15. Even though these records for highly developed turbulence are not highly intermittent, the very "spiky" nature of the process shows that the temperature (and hence refractive index) fluctuations are highly nongaussian.

Under conditions of weak or less-developed turbulence, such as would be observed on a cloudy day or at night, the intermittency is much more pronounced and may involve relatively long spatial or time scales. An example of this is shown in Fig. 16. The similarly sporadic nature of the first derivative (first increment) is also shown. However, it may be noticed that the optical and infrared scintillations do not manifest this intermittency, since they represent (weighted) averages of the turbulence field over the path. However, in the more interesting cases, the intermittency is very pronounced on the scale of a few seconds,[8] and the optical/infrared scintillations also manifest a degree of sporadicity.

Double-probe fluctuations inherently filter out the low frequency temperature components (corresponding to spatial scales greater than the probe separation), and are symmetric (Fig. 17). In the presence of substantial intermittency, this random process can be described by a fast, symmetrical, spiky process of zero mean multiplied by a slow, random envelope process.[1,8] This will be discussed further below.

Probability Distributions of Microthermal Fluctuations

Very little can be said concerning the probability distributions of the raw, single- or double-probe microthermal fluctuations (Figs. 14-17), except that the kurtosis is large. The distributions for single and double probes are shown in Fig. 18 a,b respectively; the single-probe distribution is asymmetrical as expected, while that of the double probe is basically symmetrical. In 18b, a normal distribution with the same variance is shown; the actual distribution is much more peaked around zero, and from the value of the kurtosis (21.3), the probability of large values is seen to be much greater than for the gaussian case.

Envelope Probability Distributions

In the case of pronounced intermittency, the probability distribution of the envelope function is of interest.[1,8] In order to develop this distribution, the absolute value of the two-probe fluctuations ($|\Delta T|$) is taken, and then the signal is smoothed over an averaging time of a few seconds. This results in the spectral components of the multiplicative envelope

function being developed as additive low frequencies rather than simply as narrow sidebands about the high-frequency fluctuations. The resulting distribution is approximately indicative of a bimodal distribution,[35] so that the simplest model of intermittency would be described by two discrete levels of turbulence with random transitions between them. As the averaging time is increased to many decorrelation times for the envelope, the distribution of course becomes gaussian.

"Good" Turbulence Variables

The temperature field is not a "good" characteristic of the turbulence, because it is neither stationary nor homogeneous. However, it does have stationary first increments,[36] so that, in particular, its spatial (or temporal) derivative is stationary. This will also be true of two-probe differential measurements, as long as the probe separation is not too large. These derivatives and finite differences are therefore "good" variables.

Theoretical treatments[37] have predicted that non-negative, "good" variables will exhibit log normal behavior if averaged over a spatial (or corresponding temporal) scale within the inertial subrange. A related experiment in the literature on the squared temperature derivative showed a slight skewness, which was attributed to lack of local isotropy.[38]

The squared first derivative is shown in Fig. 19 for various averaging times. The probability distribution is shown in Fig. 20, and is seen to be very similar to that of Fig. 18b, with a kurtosis of 25.6. However, the distribution of the absolute value of the derivative vs averaging time is shown in Fig. 21, and it is seen that (over the probability range covered) good log normality is exhibited for 10 msec averaging. Since the wind speed for this case was 6 m/sec, the spatial averaging scale was 6 cm--which is comfortably within the inertial subrange. Although the process retains its "log-normal-like" nature for greater and less averaging, noticeable departures from strict normality are observed.

A useful way to characterize a random process is on a "beta diagram",[34] which is a plot of (μ_4/μ_2^2) vs (μ_3^2/μ_2^3), where μ_n is a central moment of order n. This plot is shown vs averaging time in Fig. 22, for

the absolute value of the temperature derivative. The solid line indicates the locus of log normal distributions, and the point represents a gaussian distribution. It is seen that, as averaging increases, the points depart somewhat from the log normal line and converge to the gaussian point as would be expected. The departure from log normality represents an interesting and subtle manifestation of the outer scale of turbulence.

The theory of Gurvich and Yaglom[37] and the properties of log normal distributions indicate power law behavior of the moments as functions of averaging time (τ):

$$\mu_n \sim \tau^{-a_n} \tag{28}$$

where τ corresponds to spatial scales within the subrange. A plot of the first four moments of the distribution of Figs. 21 and 22 vs averaging time is shown in Fig. 23. The power law behavior is confirmed for scales within the subrange; however, the values of the exponents do not agree with the theoretical predictions.

C. Relationship Between Optical/Infrared and Microthermal Quantities

As described in Refs. 1 and 8, a major goal of this effort is to relate data spread and confidence statements for short-term-average optical/infrared measurements to corresponding microthermal quantities. To the extent that pronounced intermittency enters, the interesting averaging time for the latter (C_n^2) is on the order of a few seconds, so that fast fluctuations are removed but the intermittent envelope is not. As explained above, the C_n^2 distribution may be quasi-bimodal, and any intermittency effects showing up in the scintillations must result in a distortion of the log normality of irradiance.

Work is continuing on the necessary modelling and theoretical relationships. An empirical determination of log amplitude (scintillation) variances (σ_E^2) vs spread in microthermal C_n^2 measurements is shown in Fig. 24. The individual C_n^2 values were taken for a period of 10 seconds, and the spread and mean of a number of such values is shown for each of six runs.

Since the scintillations were measured at 10.6 μ, saturation of scintillations was not a factor; the line indicates agreement between experimental and theoretical variances, where the latter is given by[6]

$$\sigma_T^2 = 0.124\ C_n^2 k^{7/6} L^{11/6} \quad . \tag{29}$$

Similar--but much smaller--error bars could also be constructed from a sequence of measurements of σ_E^2 for each run.

It is apparent from Eq. (29) that an analytical consideration of the spread obtained in measurements of optical/infrared variances will involve spatial correlations of short-term microthermal variances (or C_n^2):

$$\text{Var}\ \sigma_E^2 \sim \left\langle C_{n_1}^2 C_{n_2}^2 \right\rangle \tag{30}$$

For this reason, arrays of portable probe systems are being employed.

D. Realizations of Random Temperature Field and Monte Carlo Simulations

In addition to analytical and empirical approaches, we intend to generate realizations or ensemble members of the random temperature field, and to employ Monte Carlo simulations of the propagation problem.

E. Physical Basis of Intermittency

The physical basis of turbulence intermittency was recently reviewed by Mollo-Christensen,[39] and the reader is referred to that paper. Turbulence, including the geophysical case, is described as occurring sporadically or in "bursts", which are episodes of generation involving energy in a nonlinear interaction through a hierarchy of (coupled) scales. These different scales of instability synergize--i.e., they interact to mutually enhance growth by extracting energy from the large scales. The higher the Reynolds number, the shorter and more intensive the bursts. The physical arguments suggest fruitful areas of microthermal experimentation, such as the simultaneous joint measure of several scales.

Of great importance in the present context is the universality of intermittency in turbulent flows; the effect of topography and altitude; and the relationship between fundamental intermittency as described here, and phenomena such as plumes.

F. Related Theoretical Issues

The basic model of the intermittent thermal field in terms of a multiplicative, low-frequency function describes a random process which has certain unusual properties. In particular,[1,8] the power spectrum and autocorrelation of the process do not exhibit the sporadicity, and e.g. averaging time analyses based on these quantities are invalidated. This raises the issue of whether or not such a process requires a more general approach from stochastic theory, and several aspects have been examined as follows:

Orthogonal Increments

The fact that the low-frequency, random, multiplicative envelope establishes narrow sidebands around each (continuum) component of the basic microthermal spectrum raises the question of suitability of the Fourier-Stieljes representation, and the orthogonality of the spectral increments.[36] We have shown that, providing the multiplicative function is stationary in the wide sense, the overall process has orthogonal increments. This conclusion will be subjected to an empirical test on the data.

Generalized Stationarity

In the above model of intermittency, there exist no additive, low-frequency components in the power spectrum of the actual microthermal process. However, such components are often physically present--e.g., in plumes, which are warmer, more turbulent regions relative to their surroundings. Such low-frequency components can cause serious problems in stochastic theory, and in fact first increments such as differential probe measurements are often utilized to avoid such stationarity questions.

The behavior of a random process at very low frequencies (the "infrared catastrophe") is treated by Mandelbrot,[40] in which he generalizes

the concept of stationarity to conditional statements, and treats "sporadic processes". However, since scintillation effects relate to turbulence components generally in the inertial subrange (hence the applicability of differential rather than single probe measurements), we believe that these low frequency components are irrelevant to our problem. This may not be entirely the case for optical infrared phase effects, which involve larger atmospheric scales.

Order and Dimension of a Random Process[36]

The "order" of a random process refers to the order of derivative or finite increment necessary for stationarity. As discussed above, the basic nature of the thermal field necessitates the use of first increments. However, it is not apparent that intermittency relates to higher "orders" as here defined.

The "dimension" of a process refers the dependence of e.g. structure functions on independent variables which are tensors. Again, it is not apparent that this relates to intermittency, although it does relate to anisotropy.

G. The Scintillation Process: Conditional Statistics, Level Crossings, Deep Fades, Markov Properties

We are interested in the conditional probability of the instantaneous irradiance at time t_2 given the value at t_1, and related issues. Unfortunately, we have empirically found the process to be non-Markovian. To the extent that the log amplitude is gaussian, however, the problem is readily tractable. Also, in order to attack the problem of deep fades in an intermittent type of process, use may be made of the theory of extreme values.[41]

H. Acknowledgments

With reference to the intermittency effort, we acknowledge ongoing collaborations with the following investigators:

Prof. Stuart Collins, Ohio State University
Dr. Peter Livingston, Naval Research Laboratory
Prof. Wm. Meecham, University of California at Los Angeles

V. Publications

During the period covered in this report, the following paper has been published:

J. R. Dunphy and J. R. Kerr, "Scintillation Measurements for Large Integrated-Path Turbulence," J. Opt. Soc. Am. 63, August 1973, pp. 981-986.

VI. References

1. "Propagation of Multiwavelength Laser Radiation through Atmospheric Turbulence," RADC-TR-73-54, January 1973, Rome Air Development Center.
2. J. R. Dunphy and J. R. Kerr, J. Opt. Soc. Am. 63, 981 (1973).
3. W. P. Brown, Jr., J. Opt. Soc. Am. 62, 966 (1972).
4. H. T. Yura, "A Physical Model for Strong Optical Amplitude Fluctuations in a Turbulent Media," submitted to J. Opt. Soc. Am.
5. S. F. Clifford, G. R. Ochs, and R. S. Lawrence, "Saturation of Optical Scintillation by Strong Turbulence," to be published.
6. R. S. Lawrence and J. W. Strohbehn, Proc. IEEE 58, 1523 (1970).
7. H. T. Yura, "Temporal-Frequency Spectrum of an Optical Wave Propagating in a Turbulent Medium Under Strong Scintillation Conditions," to be published.
8. "Propagation of Multiwavelength Laser Radiation through Atmospheric Turbulence," RADC-TR-73-164, April 1973, Rome Air Development Center.
9. J. R. Kerr and J. R. Dunphy, J. Opt. Soc. Am. 63, 1 (1973).
10. K. S. Gochelashvily, "Focused Irradiance Fluctuations in a Turbulent Medium," Optica Acta 20, 193 (1973).
11. R. F. Lutomirski and H. T. Yura, Appl. Opt. 10, 1652 (1971).
12. H. T. Yura, Appl. Opt. 10, 2771 (1971).
13. D. L. Fried and H. T. Yura, J. Opt. Soc. Am. 62, 600 (1972).
14. H. T. Yura, J. Opt. Soc. Am. 63, 567 (1973).
15. A. I. Kon, Izv. VUZ Radiofizika 13, 61 (1970).

16. D. L. Fried, J. Opt. Soc. Am. 56, 1372 (1966). D. L. Fried, Proc. IEEE 55, (1967).

17. D. L. Fried, "Effects of Atmospheric Turbulence on Static and Tracking Optical Heterodyne Receivers/Average Antenna Gain and Antenna Gain Variation, Technical Report No. TR-027, Optical Science Consultants, August 1971.

18. D. A. deWolf, "Effects of Turbulence Instabilities on Laser Propagation," RADC-TR-72-32/204, January/July 1972, Rome Air Development Center.

19. J. A. Dowling and P. M. Livingston, J. Opt. Soc. Am. 63, 846 (1973).

20. P. J. Titterton, Sylvania Electronic Systems, Inc., Mt. View, Calif., private communication.

21. D. L. Fried, J. Opt. Soc. Am. 55, 1427 (1965).

22. P. J. Titterton, Appl. Opt. 12, 423 (1973).

23. Z. I. Feizulin and Y. A. Kratsov, Izv. VUZ Radiofizika 10, 68 (1967).

24. D. L. Fried, Appl. Opt. 12, 422 (1973).

25. R. Esposito, Proc. IEEE 55, 1533 (1967).

26. J. R. Kerr and R. Eiss, J. Opt. Soc. Am. 62, 682 (1972).

27. D. L. Fried, J. Quantum Electr. QE-3, 213 (1967).

28. W. P. Brown, Jr., "Research in Interaction of Coherent Light with Solids and with Turbulent Atmospheres," Research Report, Hughes Research Laboratories, Malibu, Calif., May 1972.

29. S. A. Collins, Ohio State University, private communication.

30. S. F. Clifford, G. M. B. Bouricius, G. R. Ochs, and M. H. Ackley, J. Opt. Soc. Am. 61, 1279 (1971).

31. A. J. Huber, "Measurements of the Temporal Power Spectra of a Propagated 10.6 micron Wavefront," Technical Report, Rome Air Development Center, Spring 1973.

32. V. I. Tatarski, Propagation of Waves in a Turbulent Atmosphere, Nauka, Moscow, 1967.

33. N. E. J. Boston, "Some Features of Temperature Fluctuations in the Atmospheric Boundary Layer," presented to the American Physical Society Division of Fluid Dynamics, Annual Meeting, 22-24 November, 1971, San Diego, California.

34. G. J. Hahn and S. S. Shapiro, Statistical Models in Engineering, Wiley & Sons, p. 197, 1967.

35. R. S. Lawrence, G. R. Ochs, S. F. Clifford, J. Opt. Soc. Am. 60, 826 (1970).

36. A. M. Yaglom, An Introduction to the Theory of Stationary Random Functions, Prentice-Hall, Inc. 1962.

37. A. S. Gurvich and A. M. Yaglom, Phys. of Fluids Suppl., Boundary Layers and Turbulence, Vol. 10, Part II, pp. S59-S65, 1967.

38. C. H. Gibson, G. R. Stegen, and R. B. Willians, J. Fluid Mech. 41, 153 (1970).

39. E. Mollo-Christensen, Annual Review of Fluid Mechanics 5, 101 (1973).

40. B. Mandelbrot, "Sporadic Random Functions and Conditional Spectral Analysis: Self-Similar Examples and Limits," Proc. Fifth Berkeley Symposium on Mathematical Statistics and Probability, Vol. 3: Physical Sciences. University of California Press, Berkeley, 1967.

41. E. J. Gumbel, Statistics of Extremes, Columbia University Press, 1958.

VII. List of Figures

1. Asymptotic Log Curves for Total Angular Beamspread vs (b/ρ_o).
   a. ρ_o fixed and b varied.
   b. b fixed and ρ_o varied.

2. The Function $f(b/\rho_o)$ Inferred from the Numerical Results of Refs. 16 and 17.

3. Antenna Gains (G) vs (b/ρ_o) for Fixed ρ_o and Uniformly Illuminated Transmitter.

4. $\rho_{o_{st}}/\rho_o$ vs (b/ρ_o) from Exact and Approximate Calculations.

5. Log of Normalized Variance of Irradiance (σ_I^2):
   a. vs Log b for fixed ρ_o, $\sqrt{\frac{L}{K}}$, and σ^2
   b. vs Log ρ_o^{-1} for fixed b, $\sqrt{L/k}$, and β.

6. Power Spectrum (S) and Frequency-Weighted Power Spectrum of Transmitter Tracking (Wander) Signal.

7. Cumulative Probability Distribution of Vertical Component of Transmitter Tracking (Wander) Signal.

8. Target Irradiance at Beam Axis with 1 Second Averaging

   a. Without Wander-tracking
   b. With Wander-tracking.

9. Measured Mean Target Irradiance vs (b/ρ_o), With and Without Tracking.

10. Ratio of Measured Mean Target Irradiances With vs Without Tracking, vs b/ρ_o.

11. Power Spectra (S) of Log Amplitude Irradiance (Fading) With and Without Tracking $(b/\rho_o = 113)$.

12. Frequency Weighted Power Spectra of Log Amplitude Irradiance With and Without Tracking $(b/\rho_o = 68)$.

13. Cumulative Probability Distribution of Log Amplitude Irradiance With and Without Tracking $(b/\rho_o = 96)$.

14. Single-Probe Microthermal Fluctuations for Strong Turbulence and Low Wind Speed ($\lesssim$ 1 m/sec)

   a. 10 sec/div
   b. 1 sec/div.

15. Same as Fig. 14, for 6 m/sec Wind Speed.

16. Microthermal and Optical/Infrared Fluctuations at Night (Weak Turbulence)

   a. Single-Probe Fluctuations
   b. Square of Derivative of (a)
   c. Log Scintillations at 4880 Å
   d. Log Scintillations at 10.6 μ.

17. Double-Probe Microthermal Fluctuations for Strong Turbulence and Low Wind Speed ($\lesssim$ 1 m/sec).

18. Probability Density Function for Microthermal Fluctuations

   a. Single-Probe Fluctuations T
   b. Double-Probe Fluctuations Δ T. The Gaussian Distribution With the Same Variance is Also Shown.

19. Squared Temperature-Derivative

    a. 1 sec Averaging Time
    b. 0.1 sec Averaging Time
    c. 0.01 sec Averaging Time.

20. Probability Density Function for Temperature Derivative. The Gaussian Distribution With the Same Variance is Also Shown.

21. Cumulative Probability Distribution for Log of Absolute Value of Temperature Derivative, for Different Averaging Times.

22. β-Diagram for Absolute Value of Temperature Derivative, for Different Averaging Times. The Unaveraged, Linear Value is Also Shown.

23. First Four Moments of Absolute Value of Temperature Derivative, vs Averaging Time.

24. Experimental Log Amplitude Variance of 10.6 μ Scintillations vs Theoretical (Rytov) Value.

    Each Theoretical Value is Based on an Individual C_n^2 Measurement Taken Over a 10 sec Averaging Time. The Standard Deviation and Mean of a Number of Such Measurements is Shown for Each of Six Runs.

    Runs 1, 3, 5: Low Wind Speed
    Run 6: Essentially Zero Wind
    Runs 2, 4: Wind Speed > 4 m/sec.

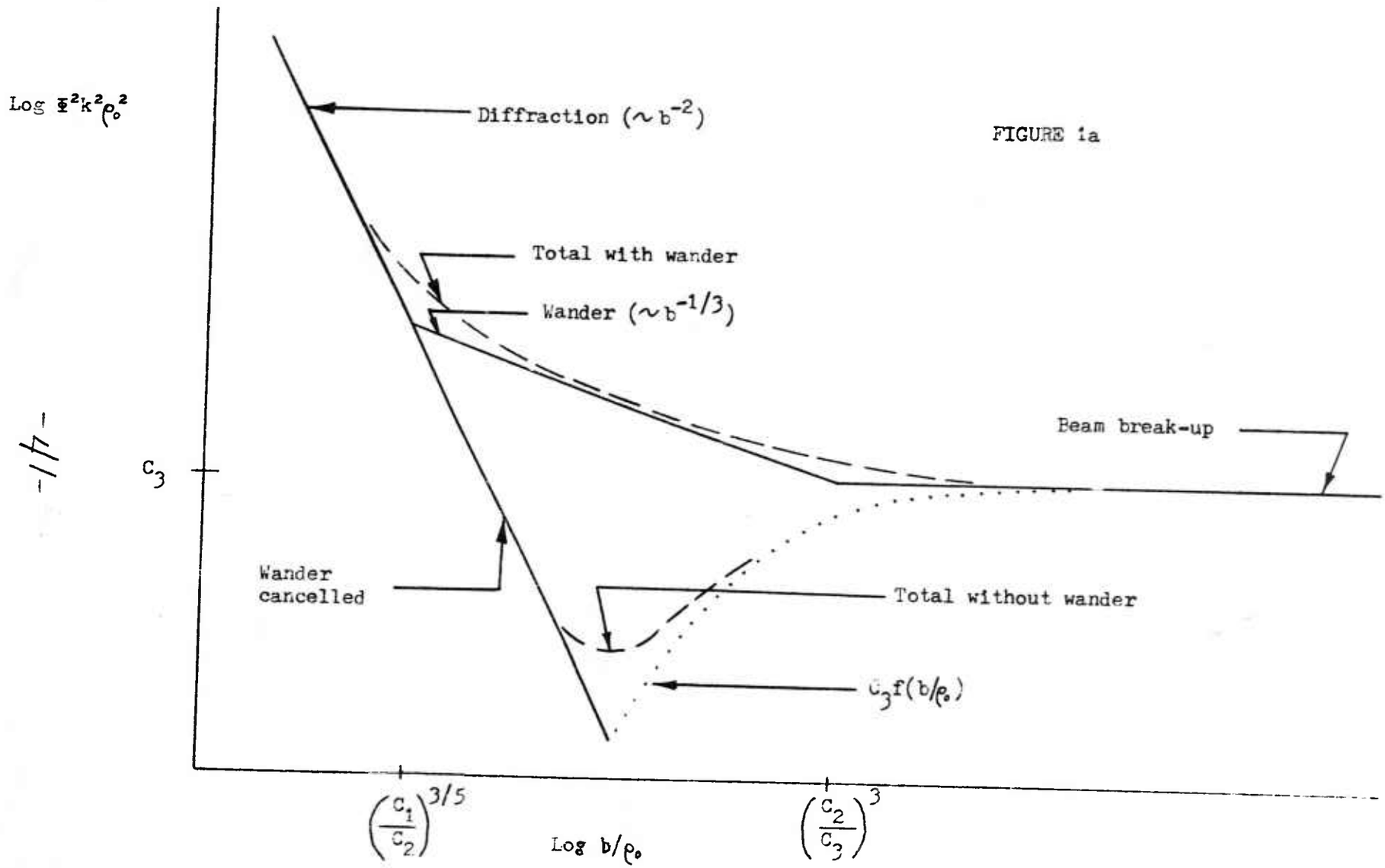
Log $\Phi^2 k^2 \rho_o^2$
Diffraction ($\sim b^{-2}$)
Total with wander
Wander ($\sim b^{-1/3}$)
Beam break-up
C_3
Wander cancelled
Total without wander
$C_3 f(b/\rho_o)$
$\left(\frac{C_1}{C_2}\right)^{3/5}$
$\left(\frac{C_2}{C_3}\right)^{3}$
Log b/ρ_o

FIGURE 1a

FIGURE 1b

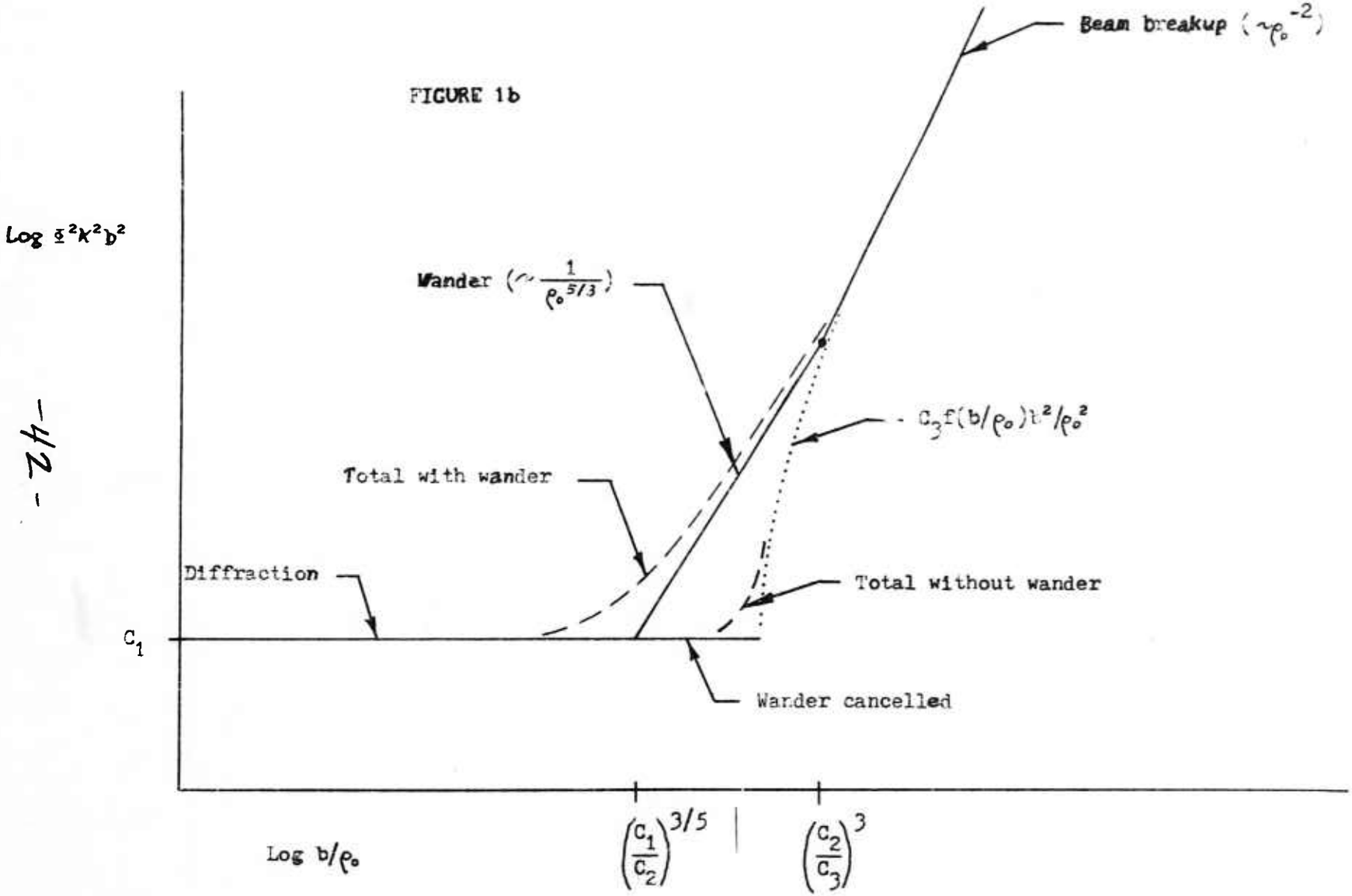
Beam breakup ($\sim \rho_o^{-2}$)
Wander ($\sim \frac{1}{\rho_o^{5/3}}$)
$C_3 f(b/\rho_o) b^2/\rho_o^2$
Total with wander
Diffraction
Total without wander
C_1
Wander cancelled
Log $\Xi^2 k^2 b^2$
Log b/ρ_o
$\left(\frac{C_1}{C_2}\right)^{3/5}$
$\left(\frac{C_2}{C_3}\right)^{3}$

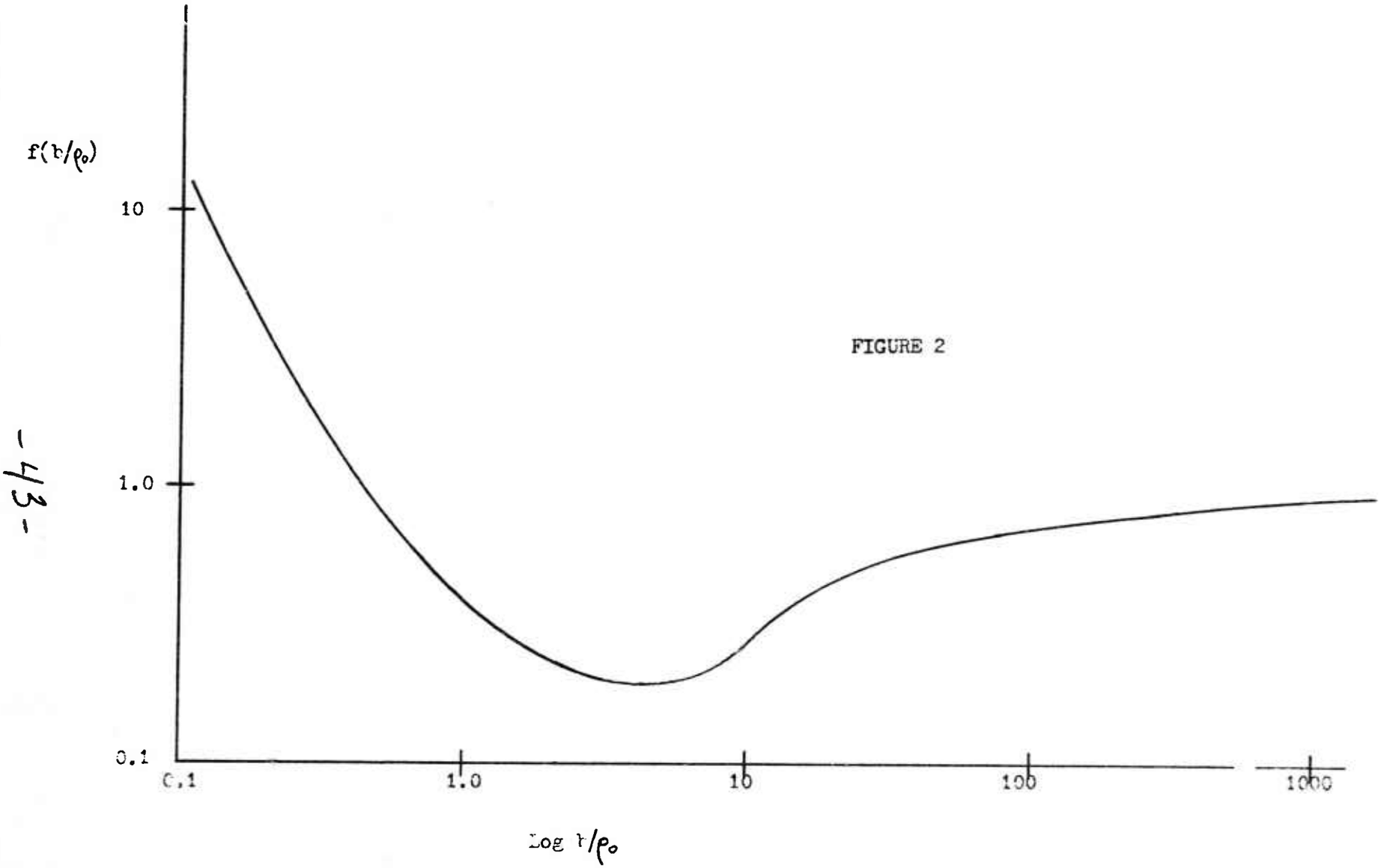

FIGURE 2

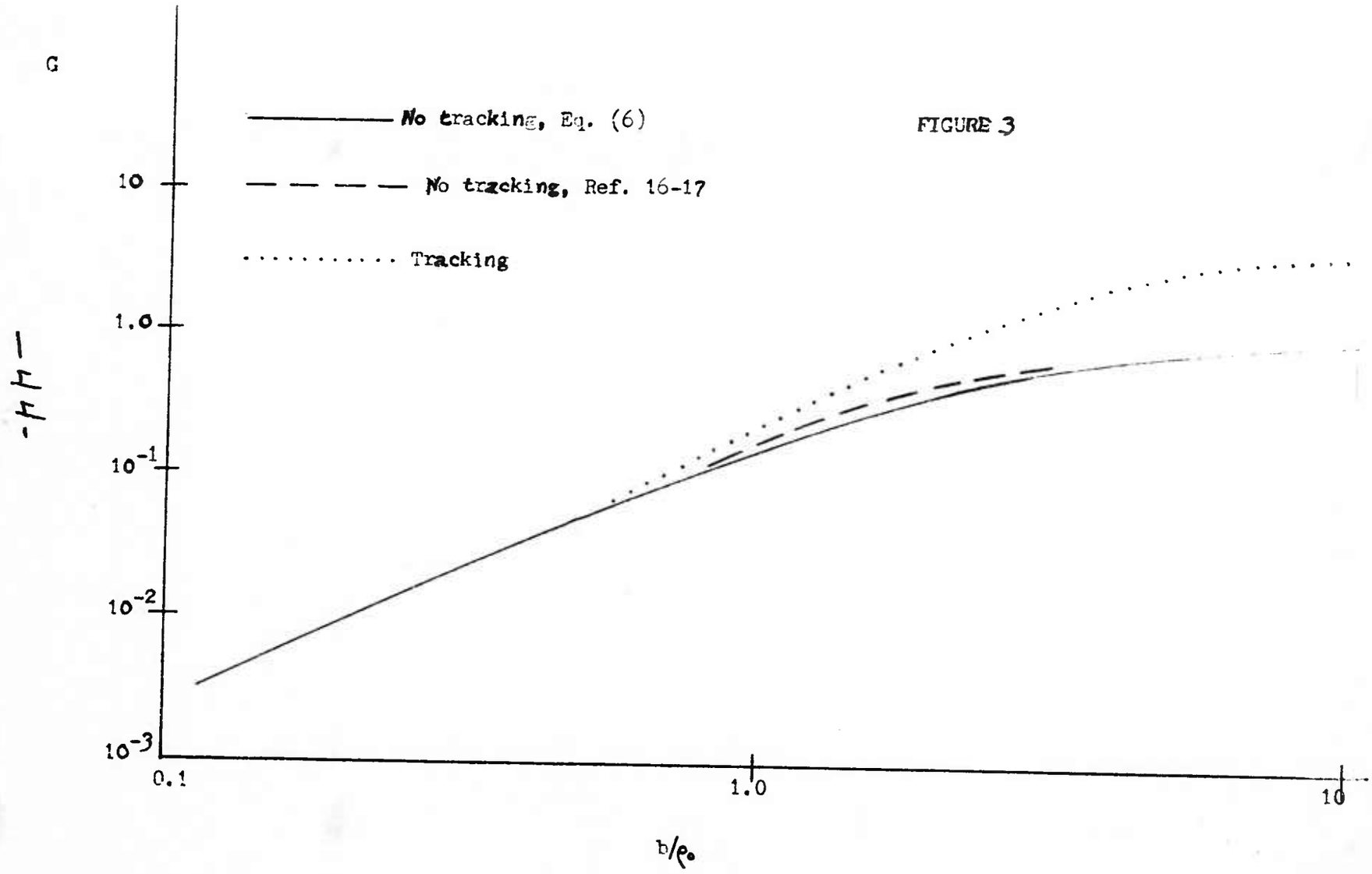
G
No tracking, Eq. (6)
No tracking, Ref. 16-17
Tracking
10
1.0
10^{-1}
10^{-2}
10^{-3}
0.1
1.0
10
b/ρ₀

FIGURE 3

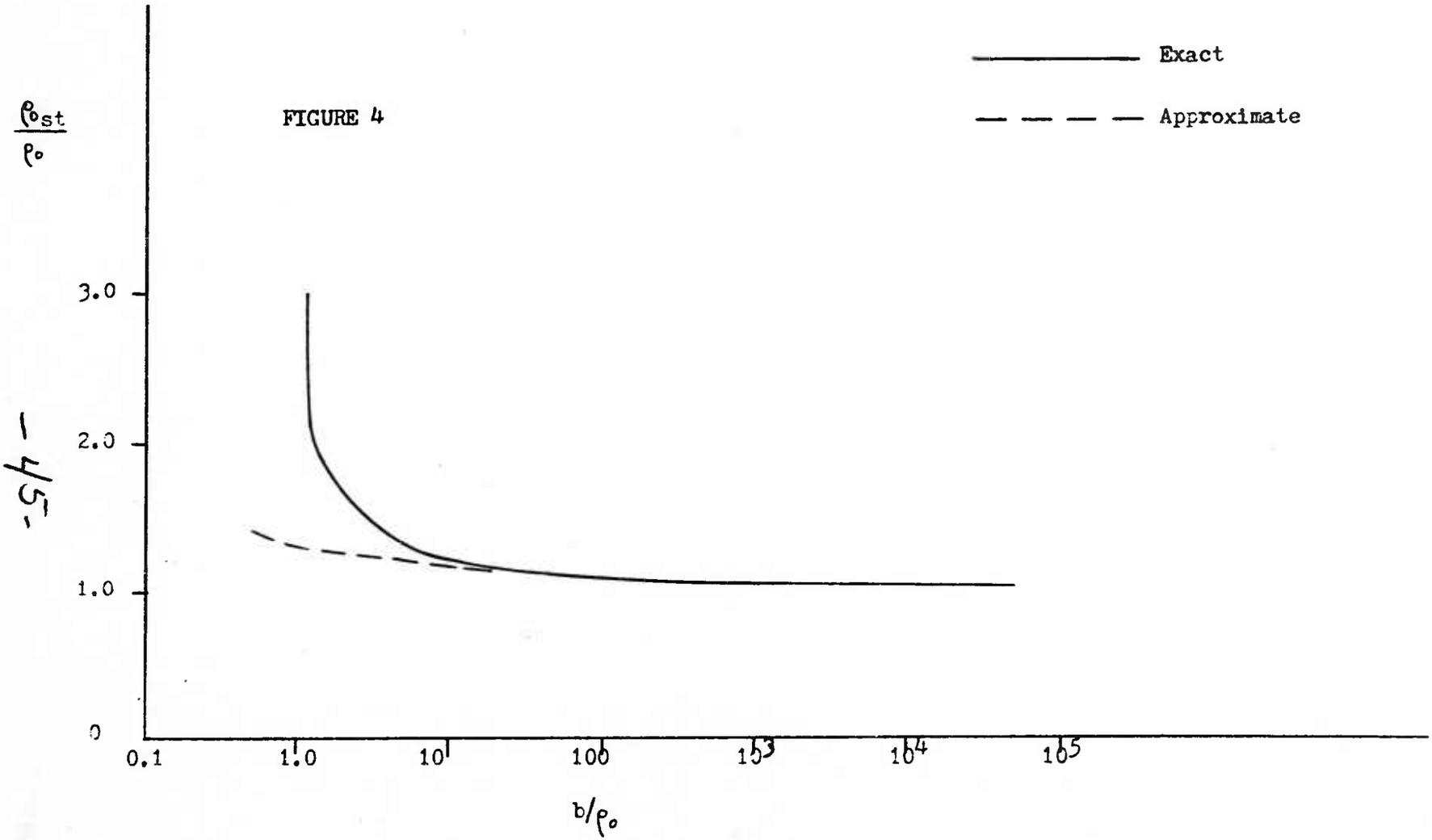
Exact
Approximate
$\frac{\rho_{0st}}{\rho_0}$
3.0
2.0
1.0
0
0.1
1.0
10
100
10^3
10^4
10^5
b/ρ_0

FIGURE 4

FIGURE 5a

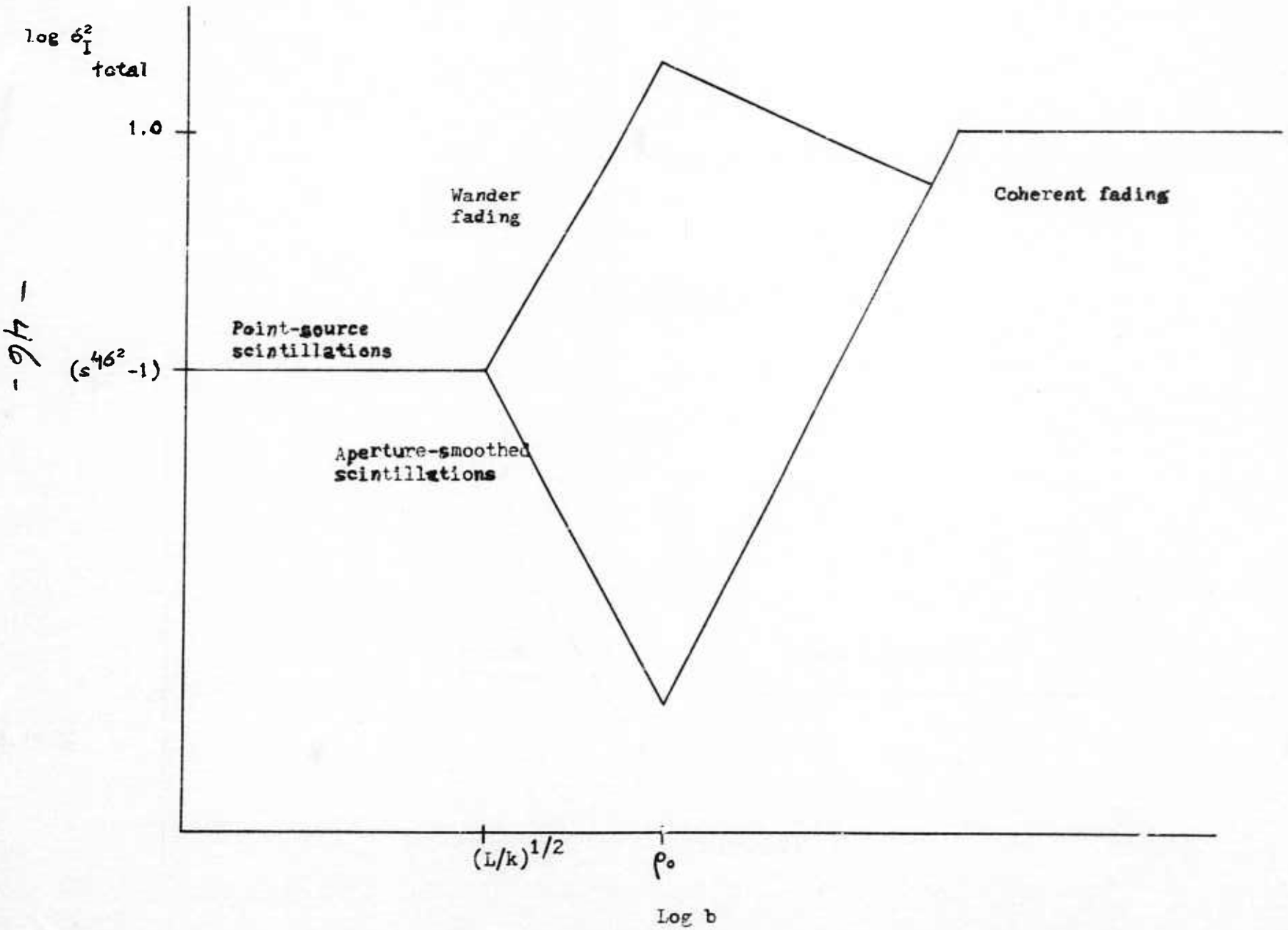
log σ_I^2 total
1.0
$(s^{4\sigma^2}-1)$
- 9/4 -
Wander fading
Coherent fading
Point-source scintillations
Aperture-smoothed scintillations
$(L/k)^{1/2}$
ρ_o
Log b

FIGURE 5b

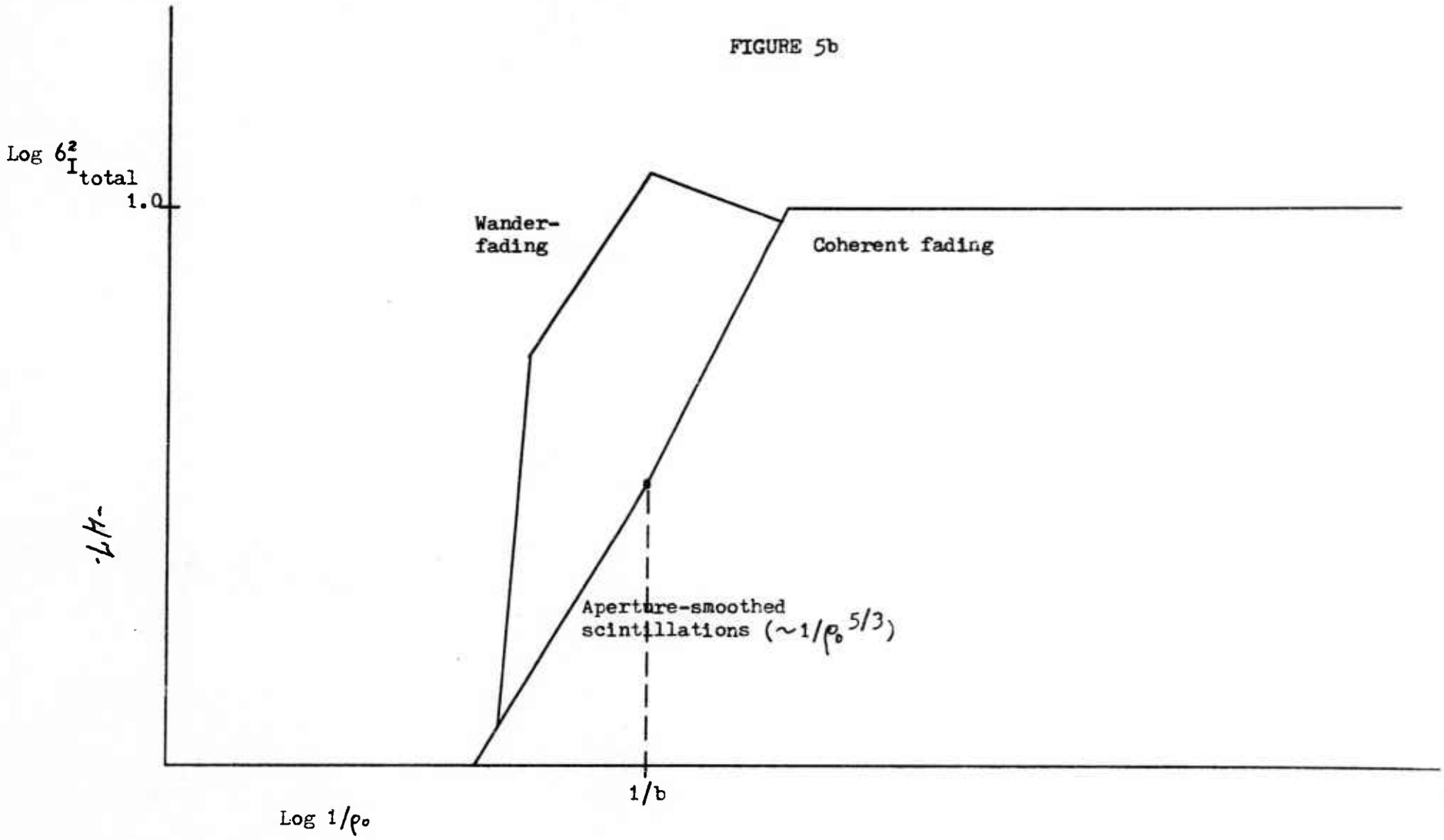
Log $6^2_{I_{total}}$
1.0
Wander-fading
Coherent fading
Aperture-smoothed scintillations ($\sim 1/\rho_o^{5/3}$)
1/b
Log $1/\rho_o$

FIGURE 6

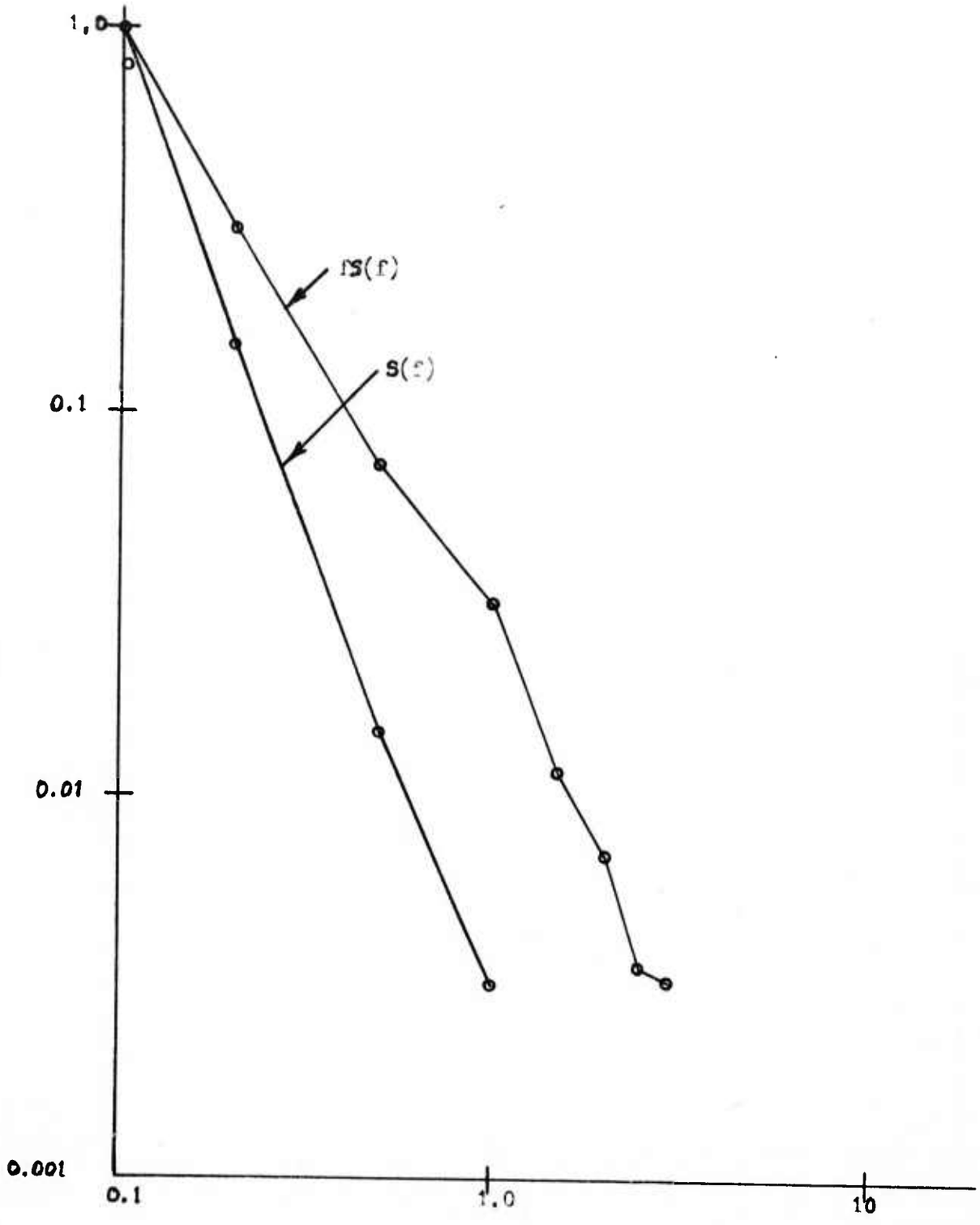

FIGURE 7

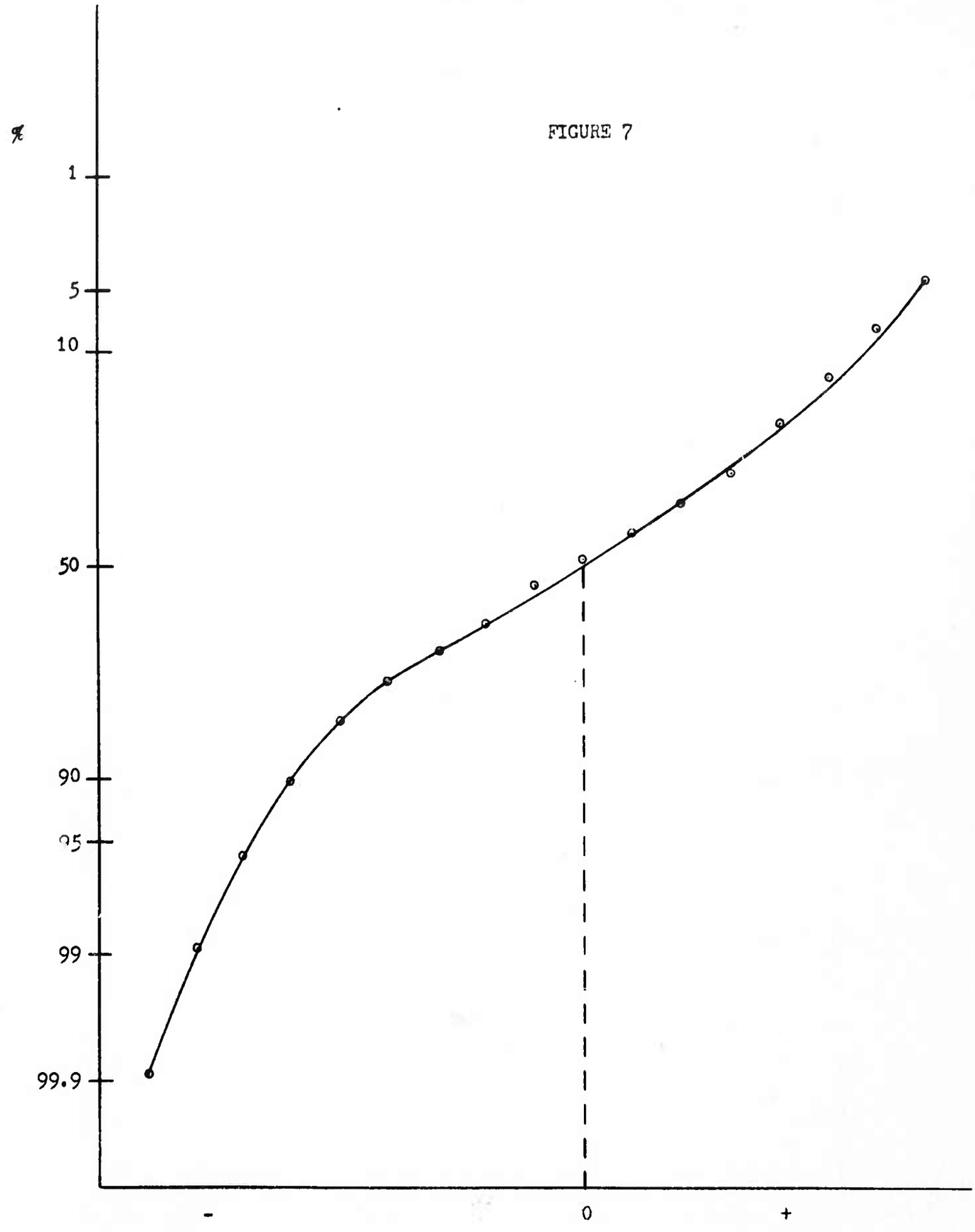

FIGURE 8a

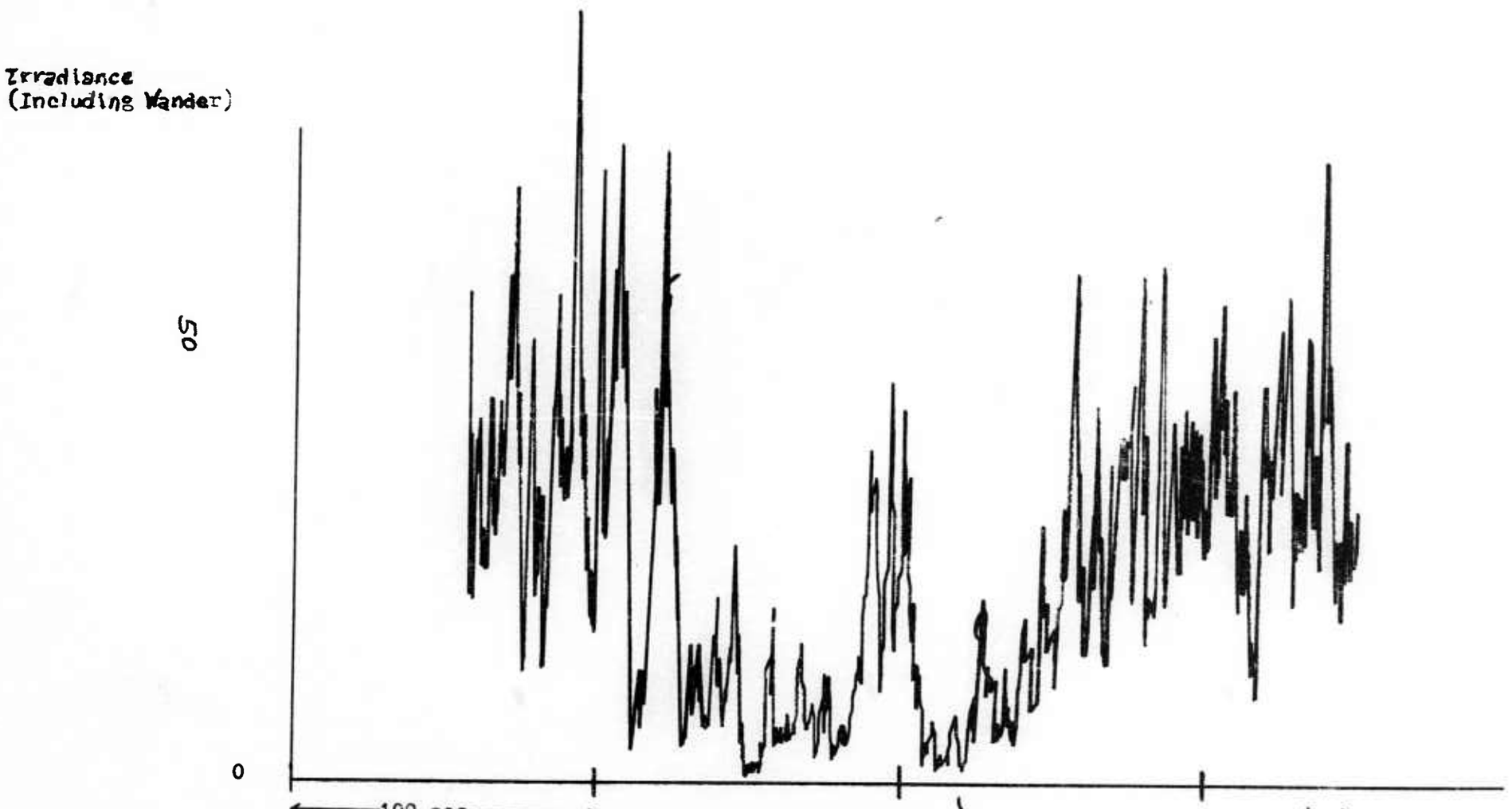

FIGURE 8b

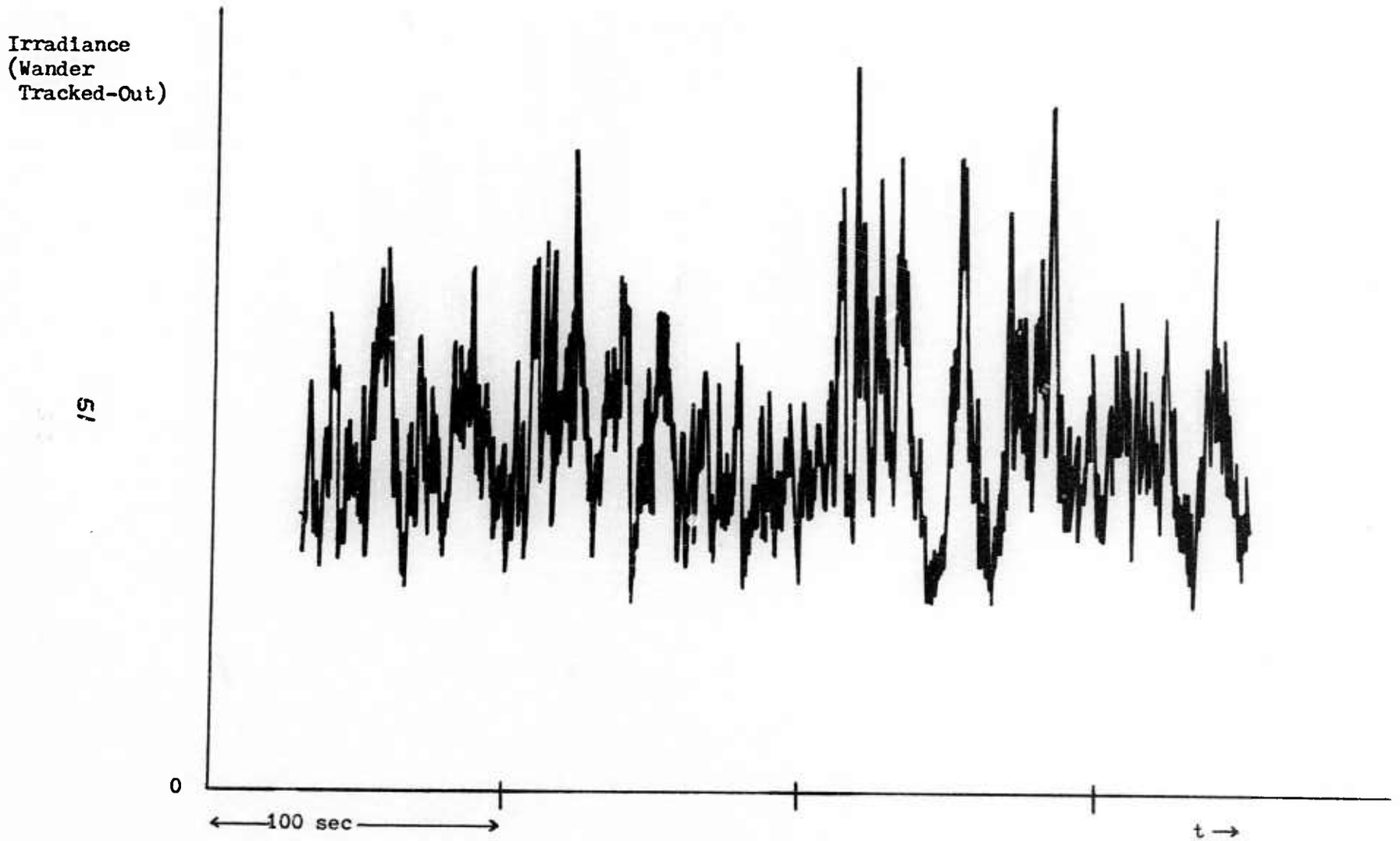

FIGURE 9

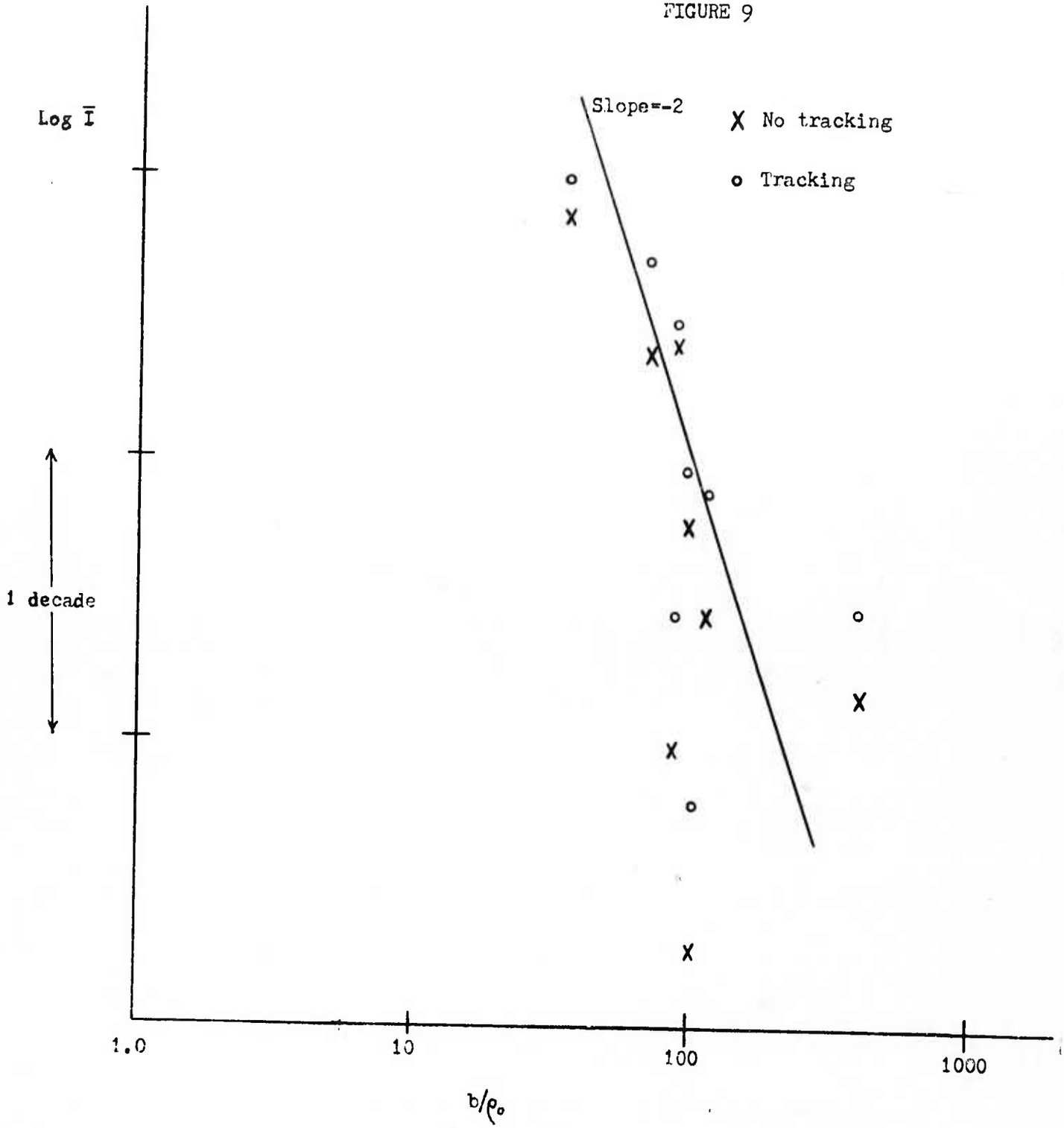
Log $\bar{I}$
Slope=-2
X No tracking
o Tracking
1 decade
1.0
10
100
1000
b/ρ₀

FIGURE 10

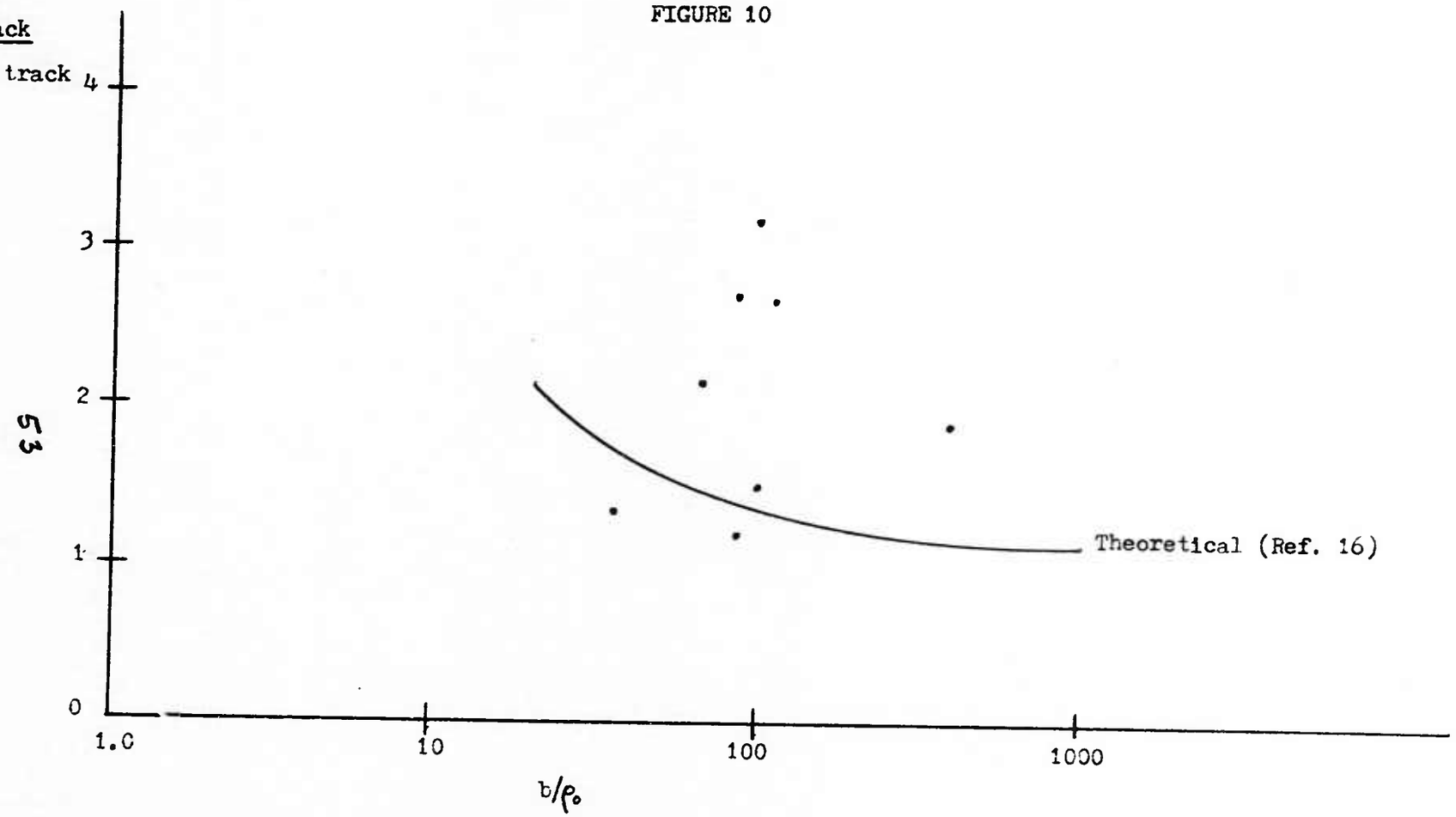
$\frac{\bar{I}_{track}}{\bar{I}_{no\ track}}$
4
3
2
1
0
1.0
10
100
1000
b/ρ₀
Theoretical (Ref. 16)

FIGURE 11

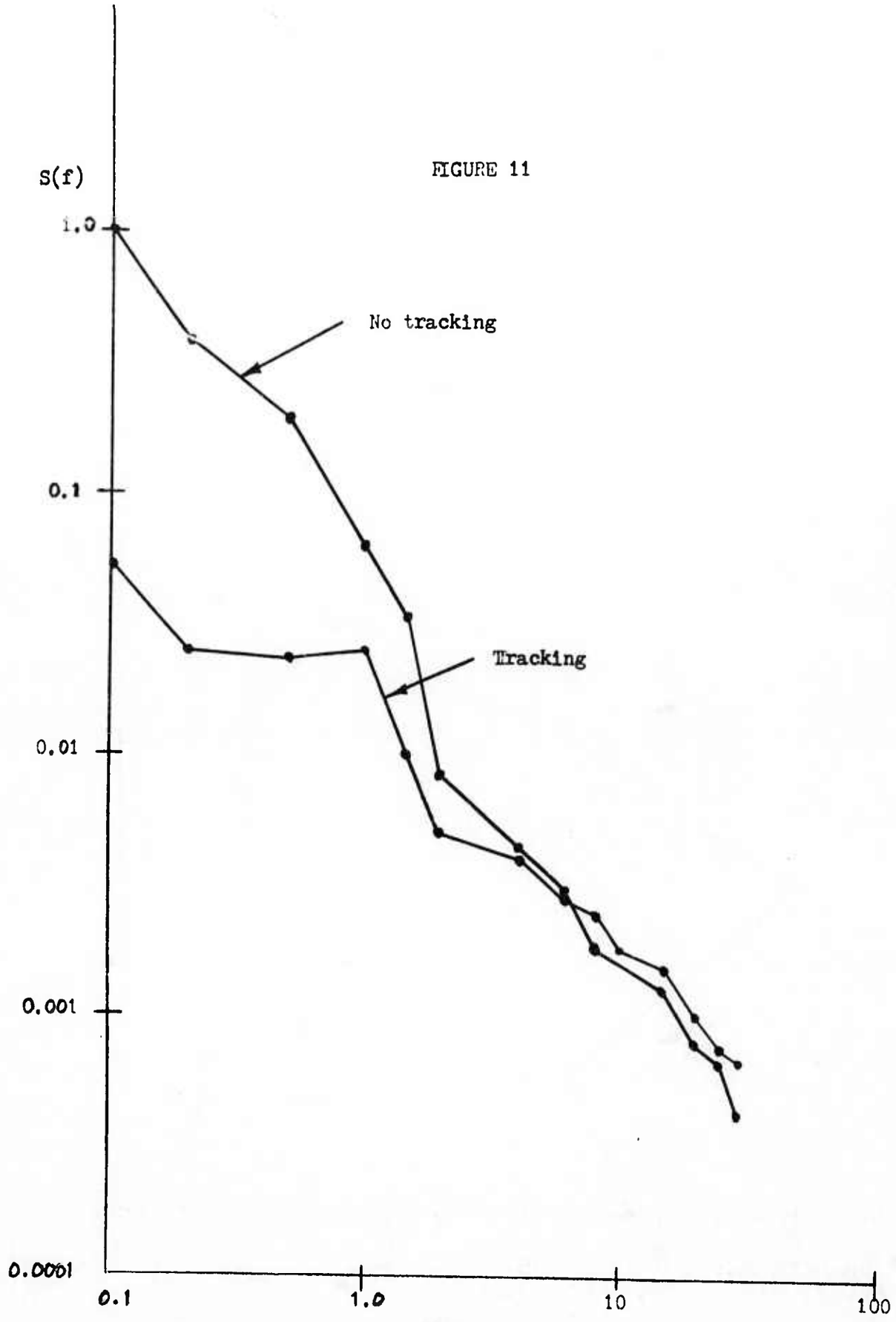

FIGURE 12

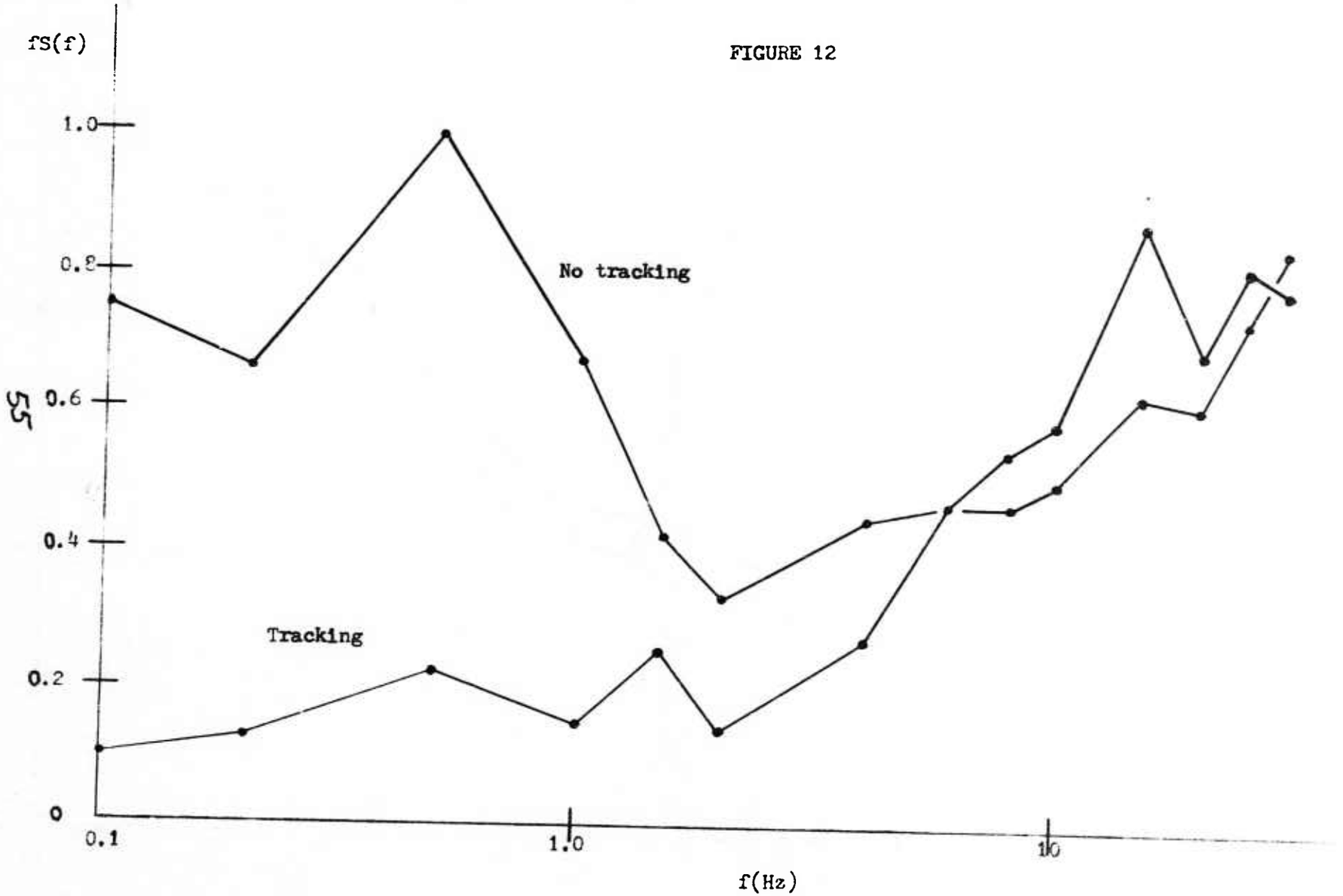

FIGURE 13

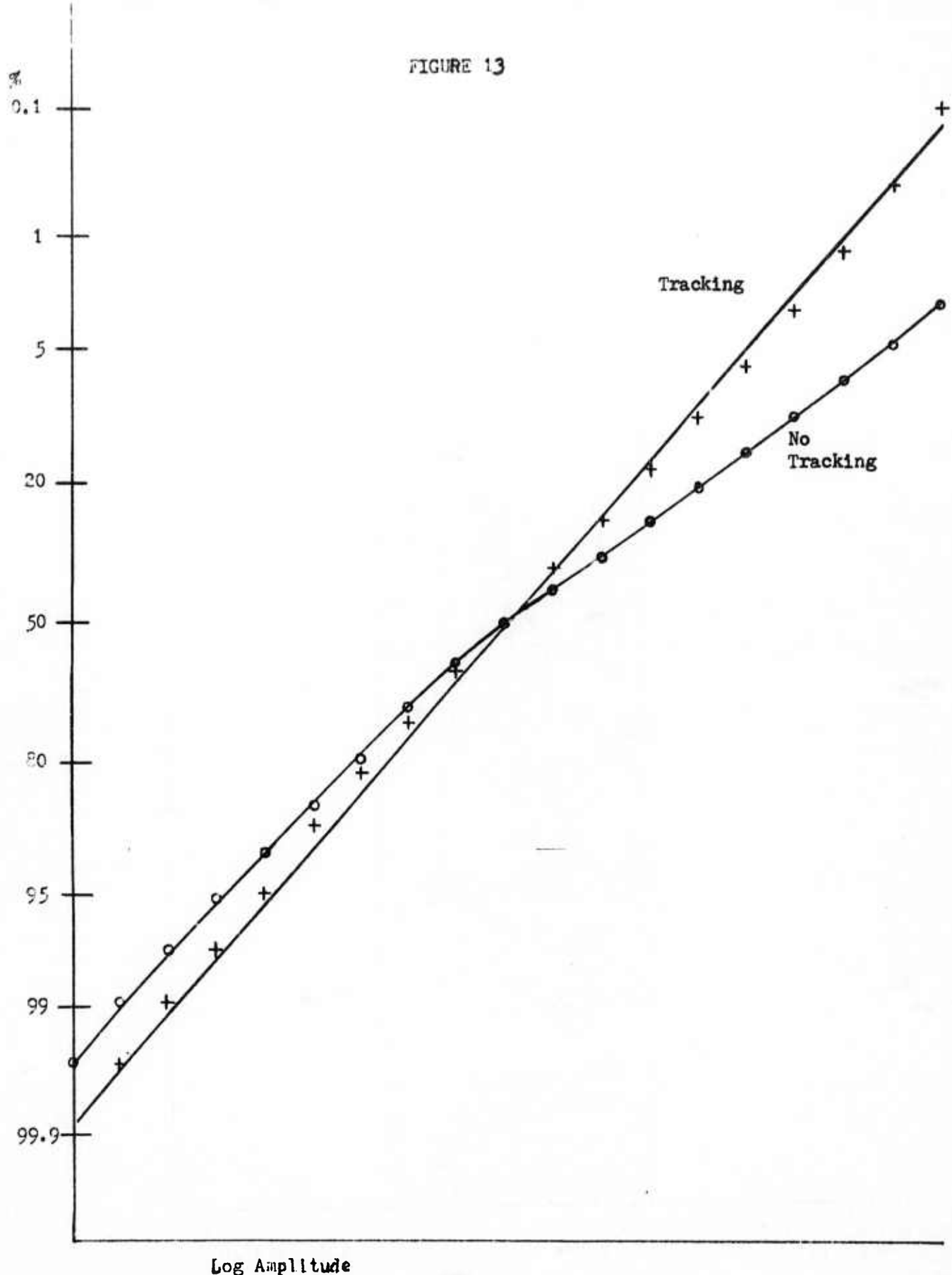

FIGURE 14a

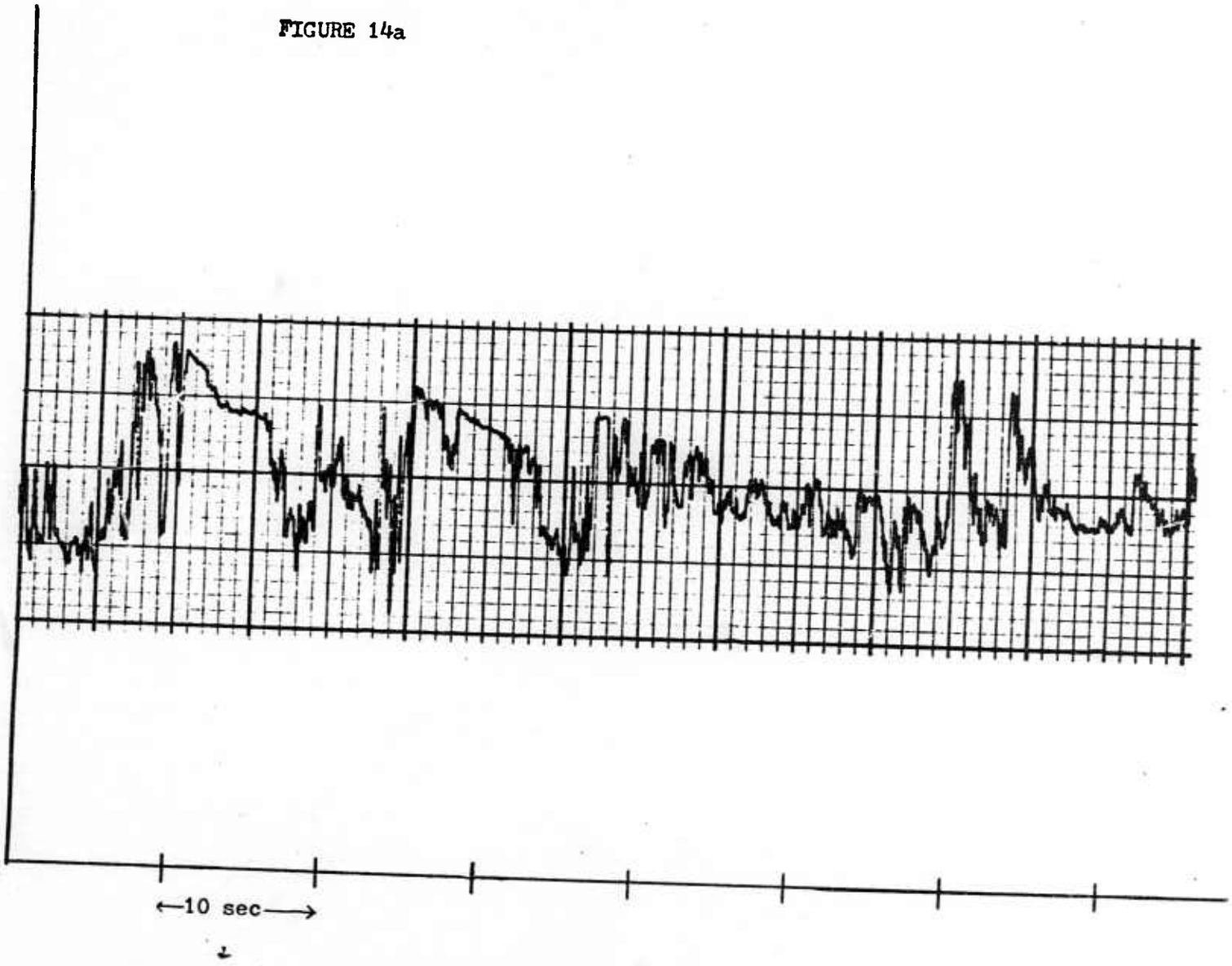

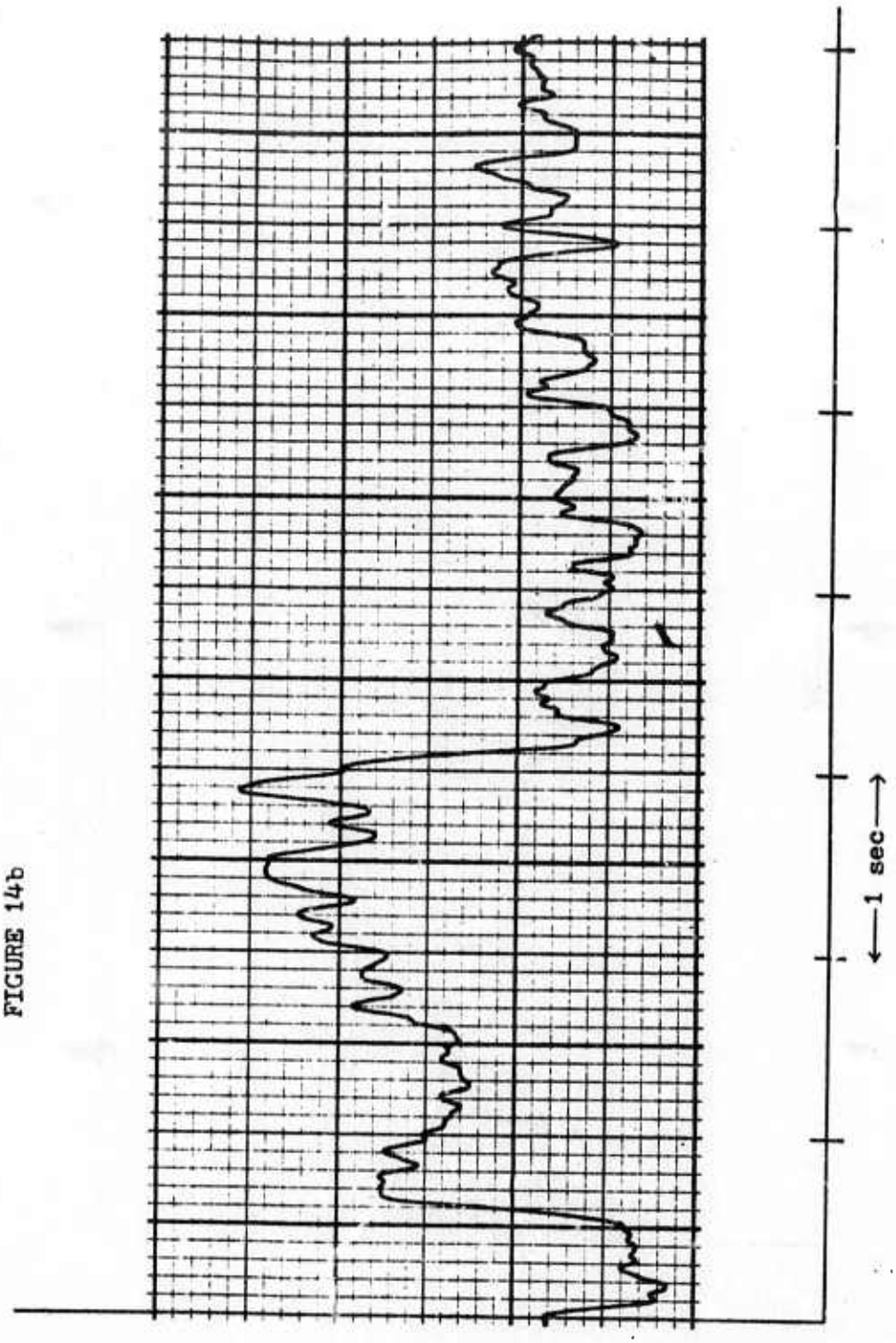

FIGURE 14b

FIGURE 15a

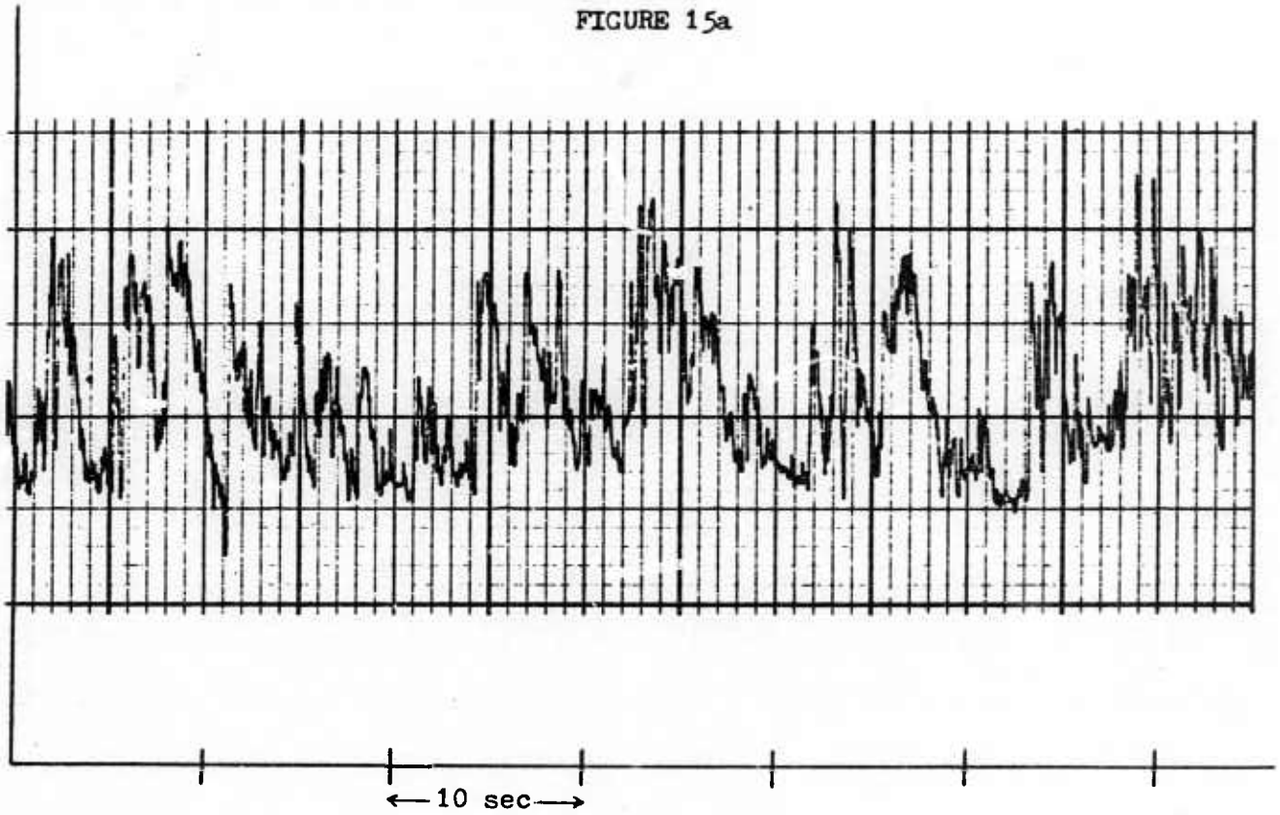

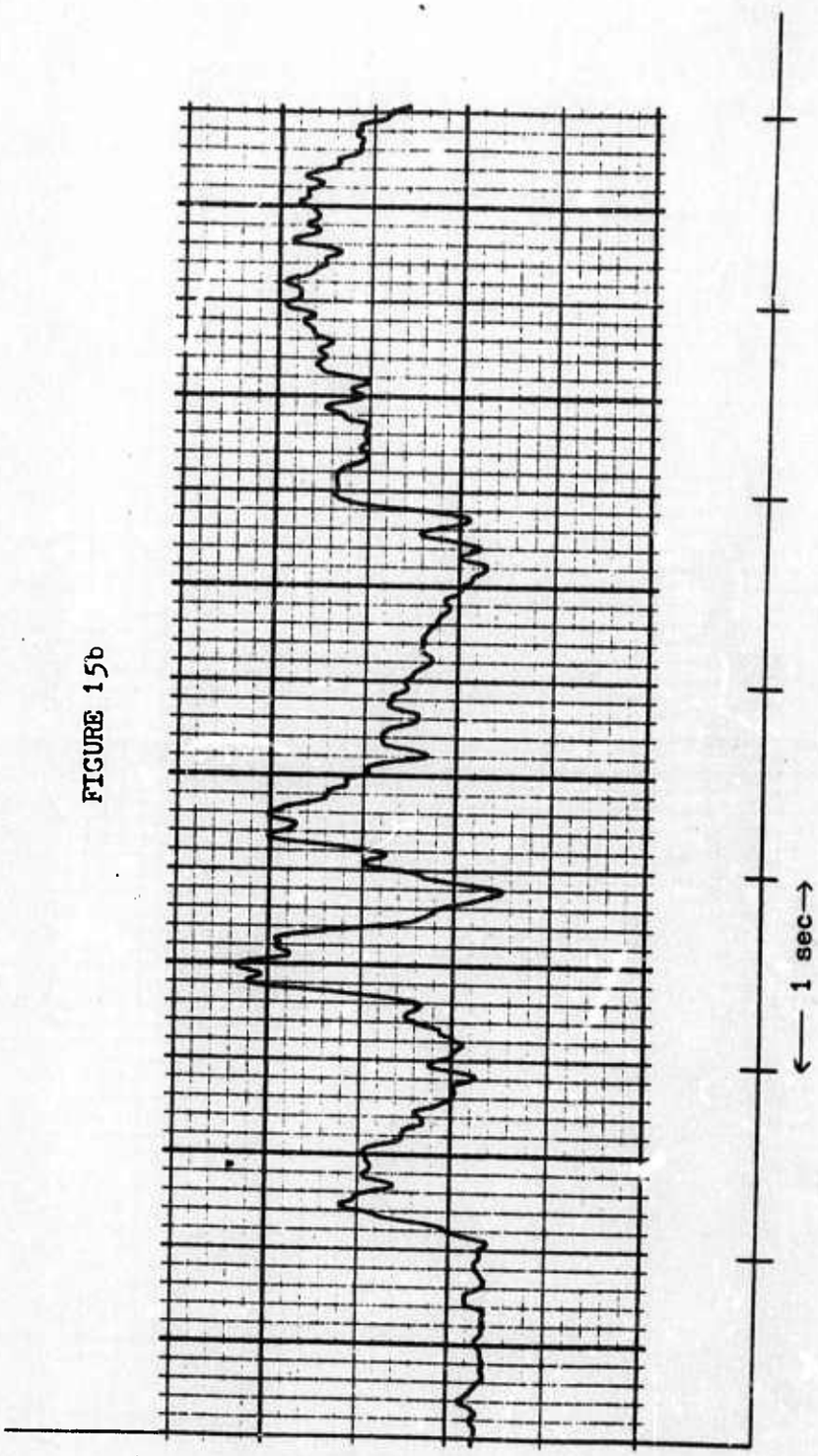

FIGURE 15b

FIGURE 16

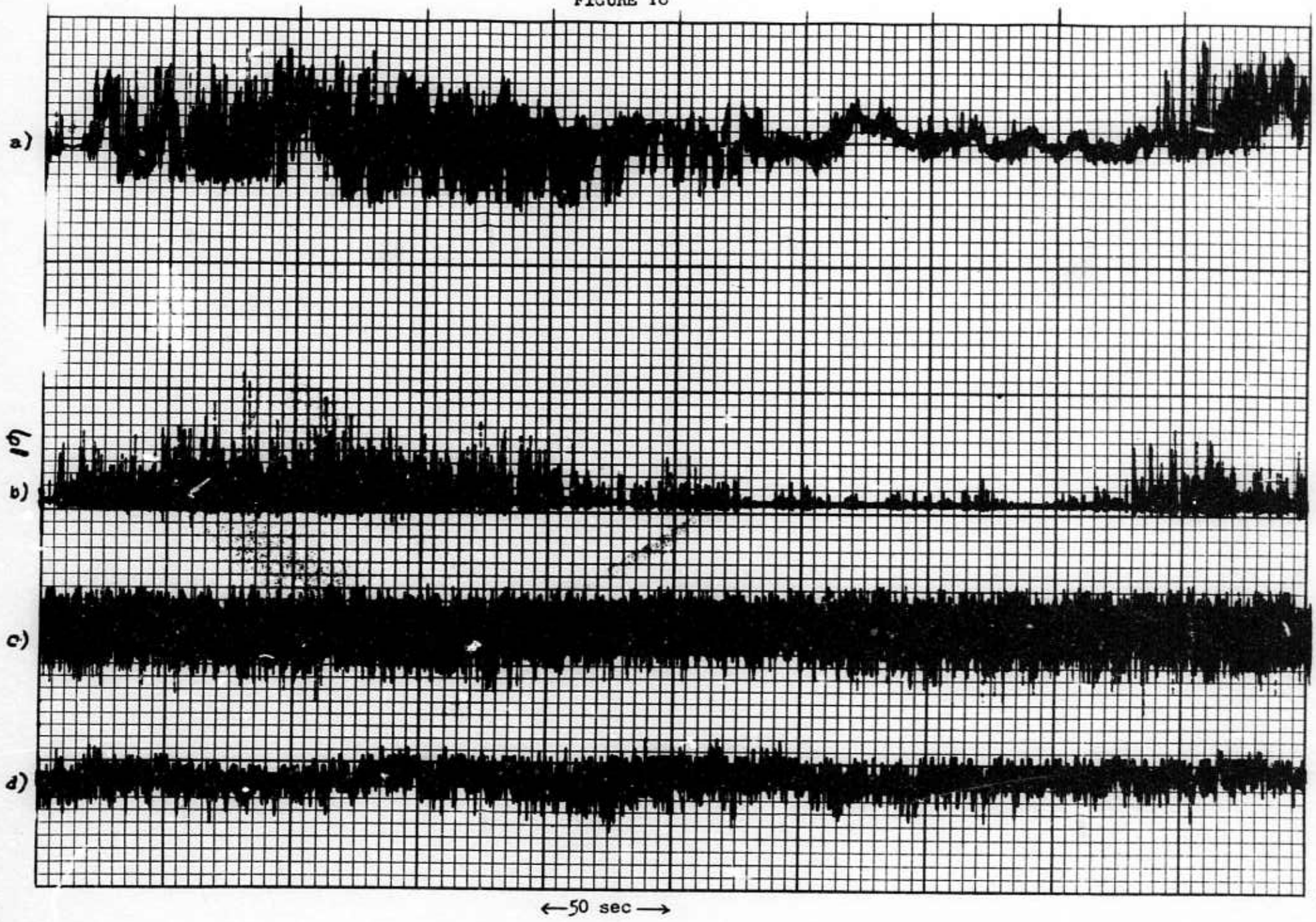

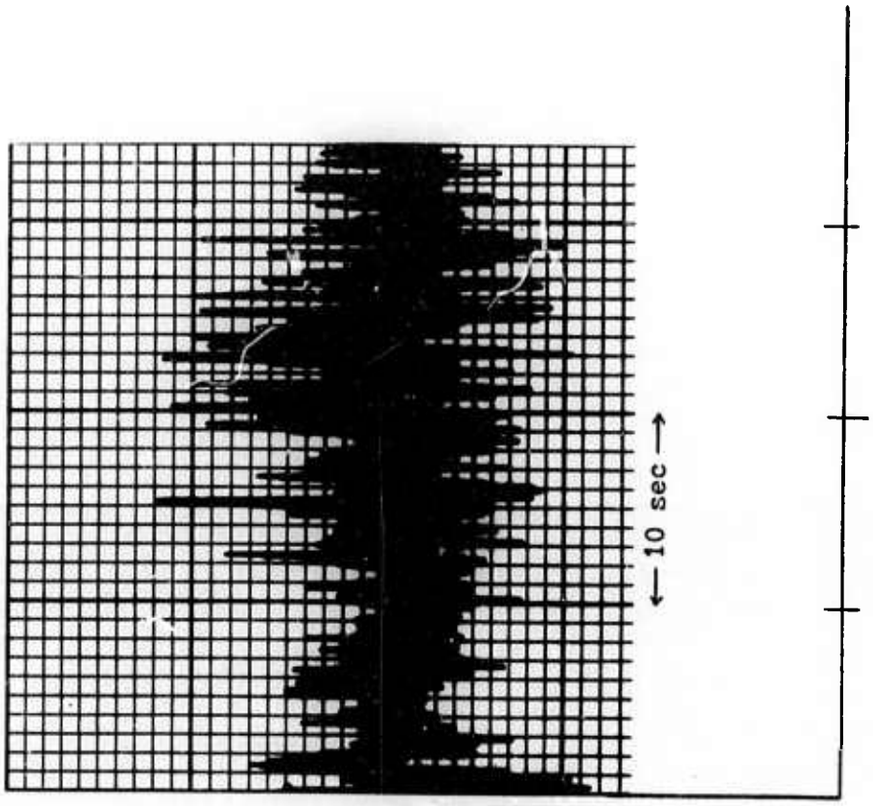

FIGURE 17

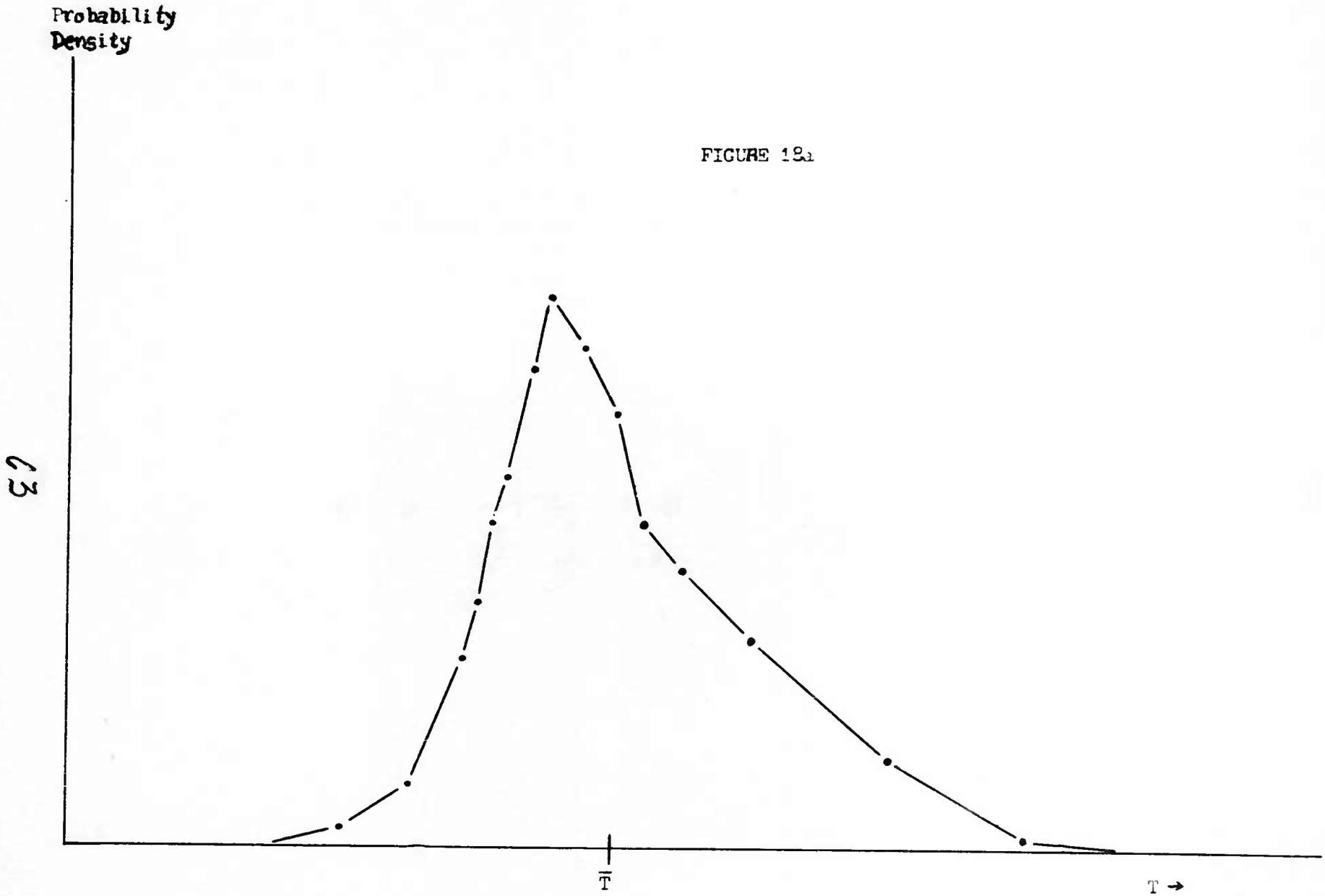

FIGURE 12a

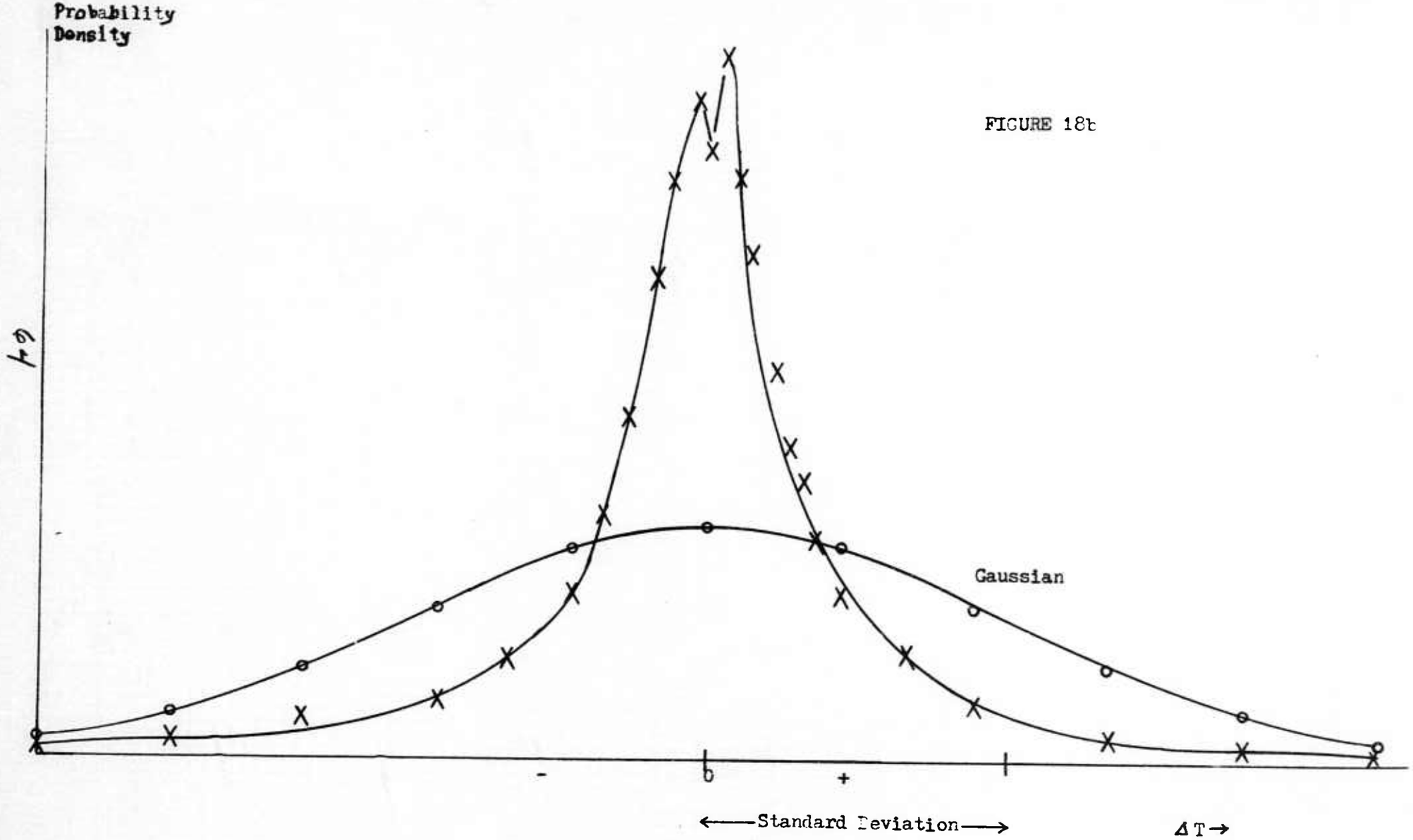

FIGURE 18b

FIGURE 19

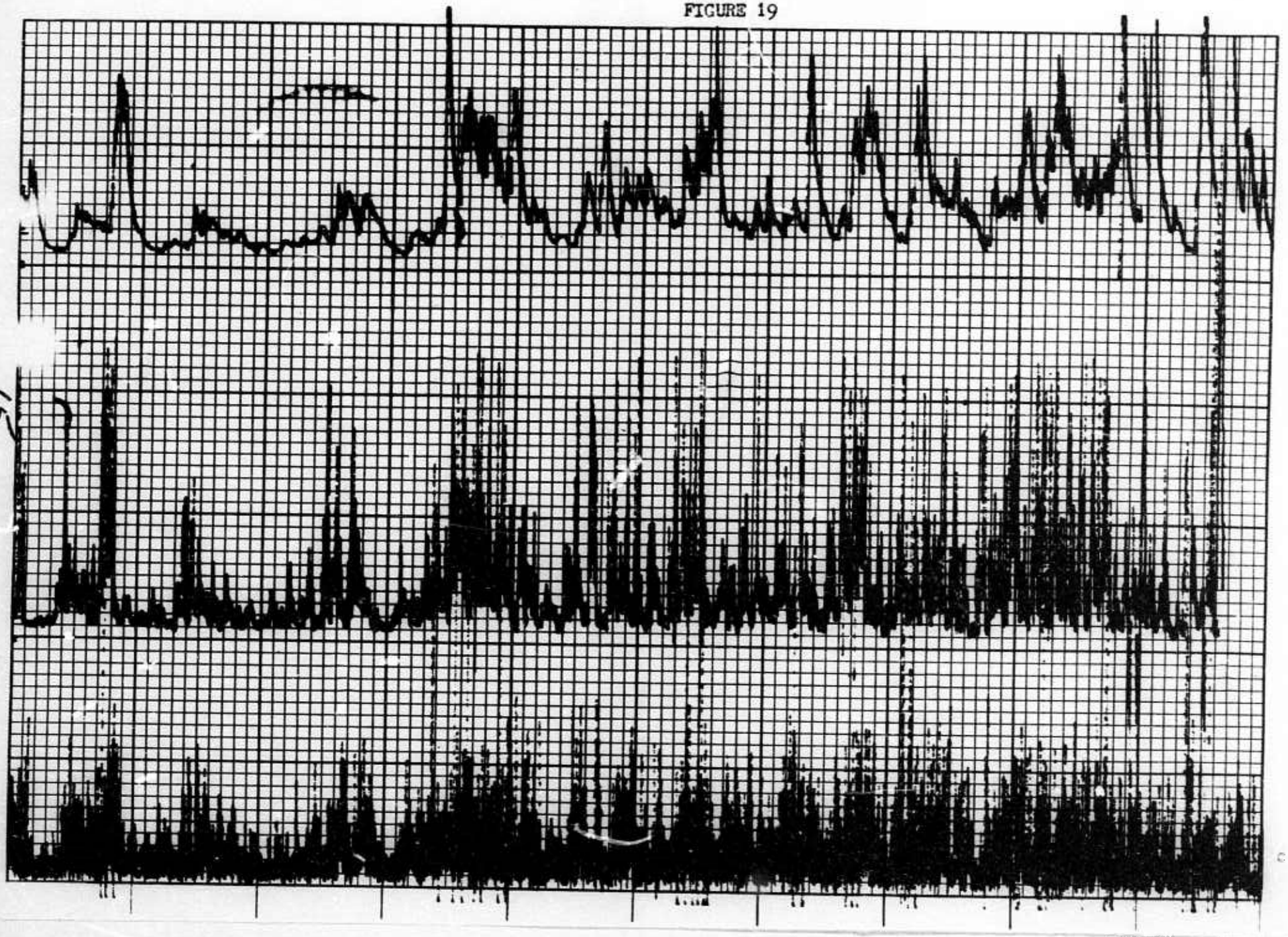

FIGURE 20

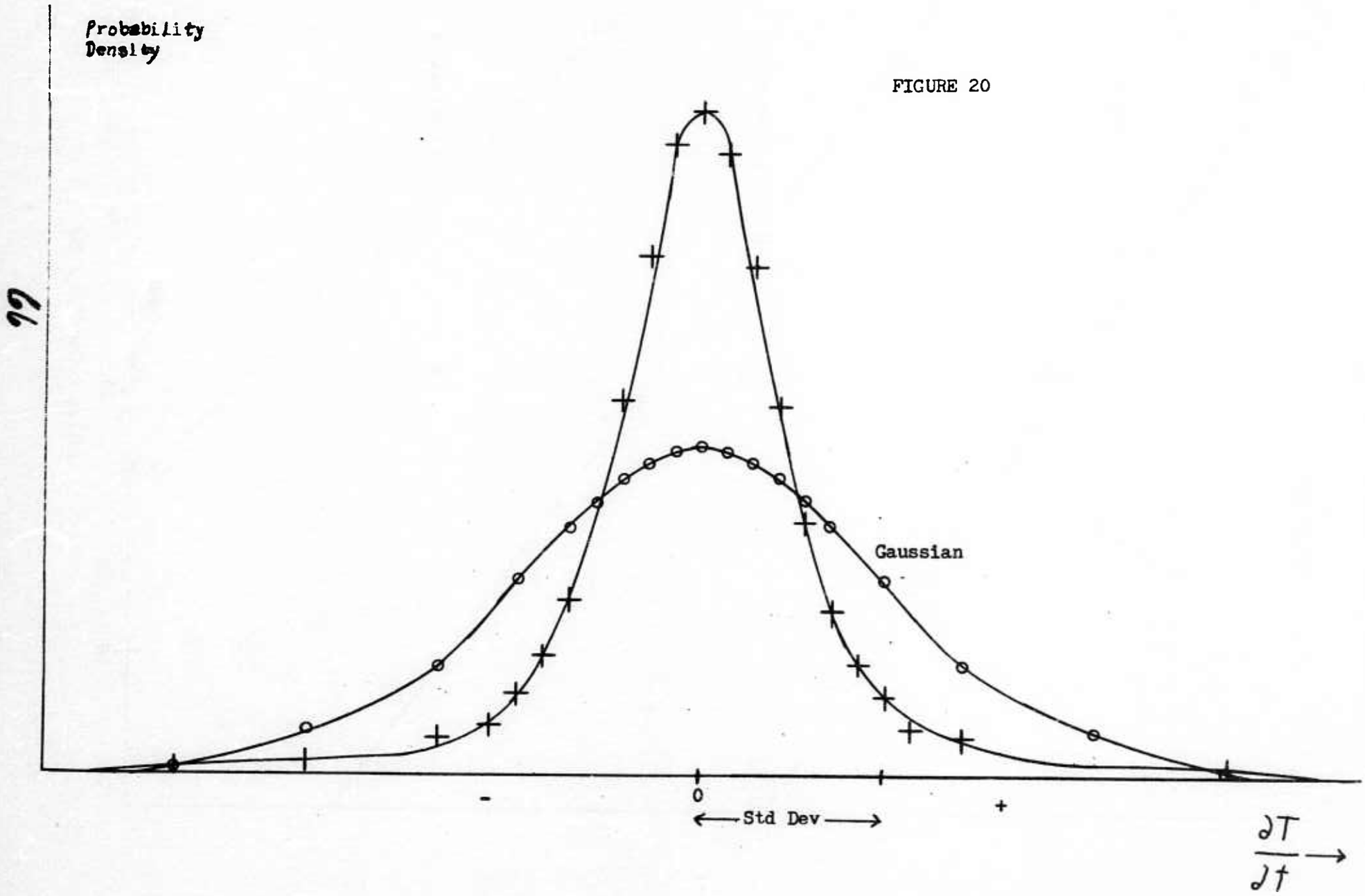

FIGURE 21

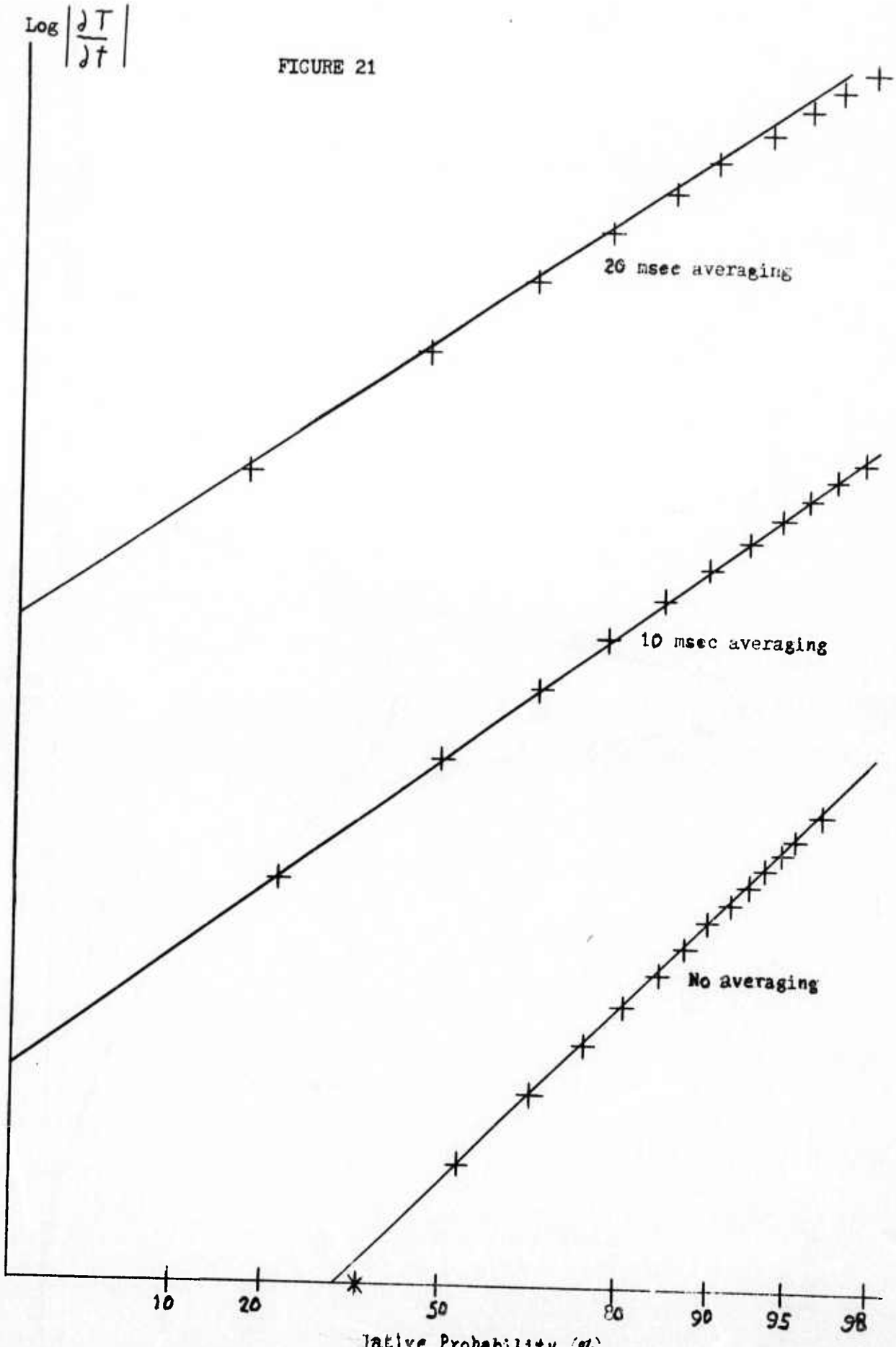
Log |∂T/∂t|
20 msec averaging
10 msec averaging
No averaging
10
20
50
80
90
95
98
lative Probability (%)

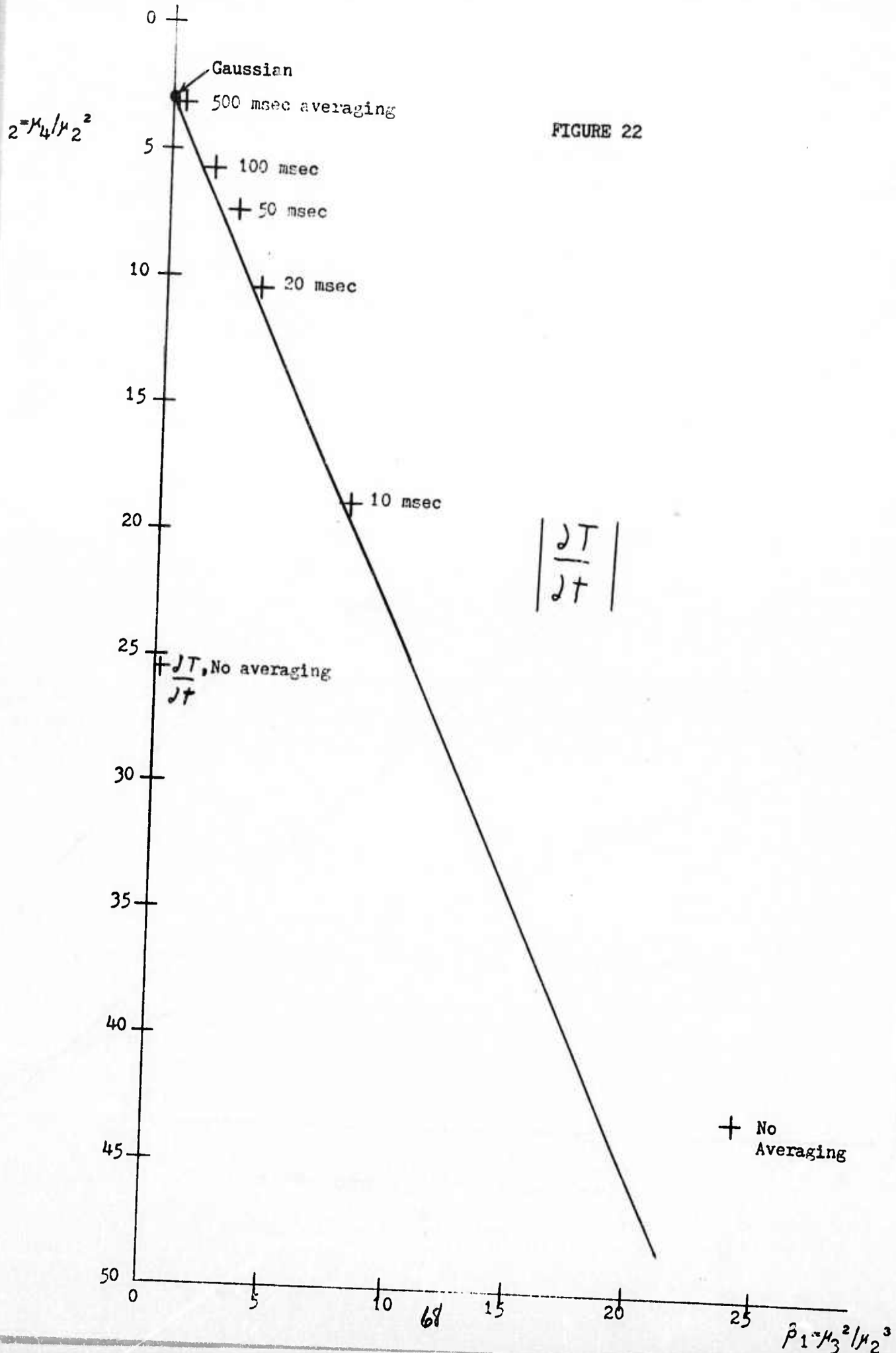
0
5
10
15
20
25
30
35
40
45
50
$2=\mu_4/\mu_2^2$
Gaussian
500 msec averaging
100 msec
50 msec
20 msec
10 msec
$\left|\frac{\partial T}{\partial t}\right|$
$\frac{\partial T}{\partial t}$, No averaging
+ No Averaging
0
5
10
15
20
25
$\beta_1=\mu_3^2/\mu_2^3$

FIGURE 22

FIGURE 23

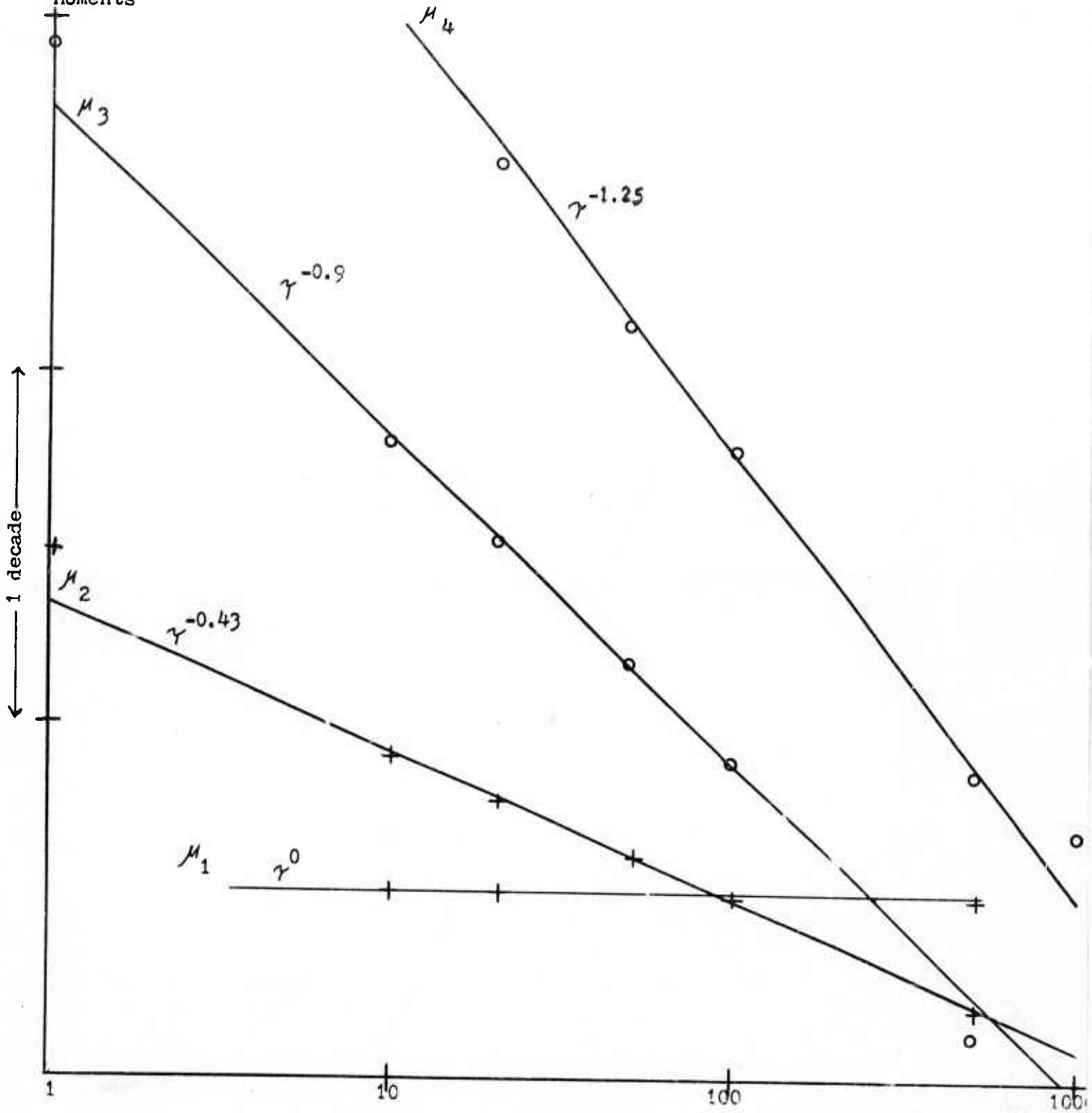

Filter Time Constant (τ), msec

FIGURE 24

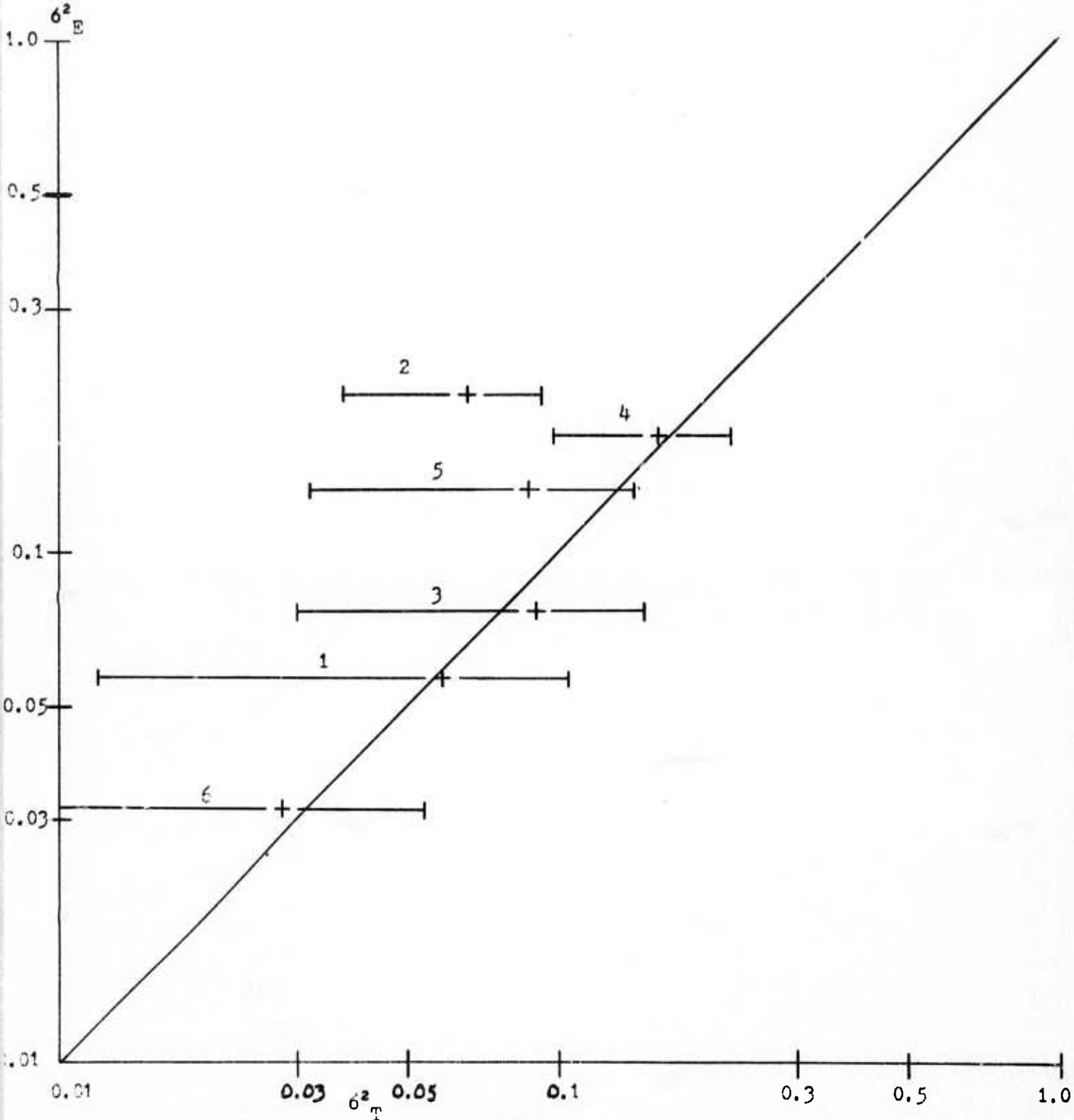
δ^2_E
1.0
0.5
0.3
0.1
0.05
0.03
.01
2
4
5
3
1
6
0.01
0.03
0.05
0.1
0.3
0.5
1.0
δ^2_T